Repository of the Max Delbrück Center for Molecular Medicine (MDC) in the Helmholtz Association

Subunit-selective NMDA receptor signaling through BRAG1 and BRAG2 during synapse maturation

Elagabani, M.N. and Brisevac, D. and Kintscher, M. and Pohle, J. and Koehr, G. and Schmitz, D. and Kornau, H.C.

Subunit-selective N-Methyl-D-aspartate (NMDA) Receptor Signaling through Brefeldin A-resistant Arf Guanine Nucleotide Exchange Factors BRAG1 and BRAG2 during Synapse Maturation[*]

Mohammad Nael Elagabani[‡§], Dušica Briševac[‡§], Michael Kintscher[‡1,2], Jörg Pohle[¶1], Georg Köhr[¶], Dietmar Schmitz[‡], and Hans-Christian Kornau[‡§3]

From the [‡]Neuroscience Research Center (NWFZ) and [§]Institute of Biochemistry, Charité - Universitätsmedizin Berlin, Charitéplatz 1, 10117 Berlin, Germany and the [¶]Central Institute of Mental Health, Medical Faculty Mannheim, Heidelberg University, 68159 Mannheim, Germany

The maturation of glutamatergic synapses in the CNS is regulated by NMDA receptors (NMDARs) that gradually change from a GluN2B- to a GluN2A-dominated subunit composition during postnatal development. Here we show that NMDARs control the activity of the small GTPase ADP-ribosylation factor 6 (Arf6) by consecutively recruiting two related brefeldin A-resistant Arf guanine nucleotide exchange factors, BRAG1 and BRAG2, in a GluN2 subunit-dependent manner. In young cortical cultures, GluN2B and BRAG1 tonically activated Arf6. In mature cultures, Arf6 was activated through GluN2A and BRAG2 upon NMDA treatment, whereas the tonic Arf6 activation was not detectable any longer. This shift in Arf6 regulation and the associated drop in Arf6 activity were reversed by a knockdown of BRAG2. Given their sequential recruitment during development, we examined whether BRAG1 and BRAG2 influence synaptic currents in hippocampal CA1 pyramidal neurons using patch clamp recordings in acute slices from mice at different ages. The number of AMPA receptor (AMPAR) miniature events was reduced by depletion of BRAG1 but not by depletion of BRAG2 during the first 2 weeks after birth. In contrast, depletion of BRAG2 during postnatal weeks 4 and 5 reduced the number of AMPAR miniature events and compromised the quantal sizes of both AMPAR and NMDAR currents evoked at Schaffer collateral synapses. We conclude that both Arf6 activation through GluN2B-BRAG1 during early development and the transition from BRAG1- to BRAG2-dependent Arf6 signaling induced by the GluN2 subunit switch are critical for the development of mature glutamatergic synapses.

Although fast excitatory neurotransmission in the central nervous system is mediated by synapses containing both AMPARs[4] and NMDARs, developing synapses are often AMPAR-silent and rely on NMDARs only (1). NMDARs govern the functional maturation of glutamatergic synapses as well as activity-dependent alterations of their strength by changing membrane trafficking that affects the AMPAR content of the postsynaptic membrane (2).

NMDARs assemble as tetramers from two GluN1 and two GluN2/GluN3 subunits (2). A variety of four GluN2 subunits forms the basis for the functional diversity of the receptor. Whereas embryonic NMDARs contain GluN2B or GluN2D, GluN2A is increasingly expressed only during postnatal development (3–5) and incorporated into NMDARs of synapses receiving a strong activity (6). This developmental GluN2 subunit switch prevents premature formation of synapses but allows synapse maturation at sites of strong input (7–9). GluN2 subunits possess large intracellular domains and interact directly or indirectly with core components of the postsynaptic density (PSD) including PSD-95 family proteins and a number of signaling molecules including kinases, phosphatases, GTPases, and their regulators (10). The NMDAR channel mediates influx of calcium ions that act as second messenger molecules within the dendritic spine and are intimately coupled to neuronal plasticity processes (2).

Among the proteins strongly enriched in the PSD are BRAG1 and BRAG2, two closely related guanine nucleotide exchange factors (GEFs) for the small GTPase Arf6 (11–14). BRAG proteins contain a Sec7 domain catalyzing the GDP-GTP exchange in tandem with a pleckstrin homology domain and an IQ-like motif that binds calcium-free calmodulin (15). Arf6 regulates membrane trafficking and actin cytoskeleton remodeling at the

---

[1] Both authors contributed equally to this work.

[2] Present address: Laboratory of Synaptic Mechanisms, Brain Mind Inst., School of Life Science, École Polytechnique Fédérale de Lausanne, 1015 Lausanne, Switzerland.

[3] Recipient of a *Chica and Heinz Schaller* (CHS) short term fellowship from the CHS Stiftung and a Heisenberg fellowship (KO 2290/1-1) from the Deutsche Forschungsgemeinschaft. To whom correspondence should be addressed: Neuroscience Research Center (NWFZ), Charité - Universitätsmedizin Berlin, Charitéplatz 1, 10117 Berlin, Germany. Tel.: 49-30-450-539131; E-mail: hckornau@charite.de.

---

[4] The abbreviations used are: AMPAR, α-amino-3-hydroxy-5-methyl-4-isoxazolepropionic acid (AMPA) receptor; aa, amino acids; AAV, adeno-associated virus; Arf6, ADP-ribosylation factor 6; BRAG, brefeldin A-resistant Arf guanine nucleotide exchange factor; ctrl, control; CV, coefficient of variation; D-AP5, D-(−)-2-amino-5-phosphonopentanoic acid; DIV, day *in vitro*; E, embryonic day; GEF, guanine nucleotide exchange factor; GGA3, Golgi-associated, γ-adaptin ear-containing, Arf-binding protein 3; KD, knockdown; LTD, long term depression; mEPSC, miniature excitatory postsynaptic current; NMDAR, N-methyl-D-aspartate (NMDA) receptor; P, postnatal day; pd, pulldown; PSD, postsynaptic density; R_s, series resistance; t, total; VGLUT 1, vesicular glutamate transporter 1.

plasma membrane (16, 17). Experiments in primary neuronal cultures indicated that Arf6 influences the maturation and maintenance of dendritic spines (18, 19) and that a significant fraction of AMPARs recycles through Arf6-positive endosomes (20).

BRAG proteins have been implicated in neuronal development and plasticity (21). Mutations in the gene for BRAG1 were identified as the cause of X chromosome-linked intellectual disability in several families (22). Viral expression of BRAG1 in hippocampal slice cultures reduced evoked AMPAR currents depending on endogenous NMDAR activity (15). We found BRAG2 to be involved in different forms of long term depression (LTD) in the mouse hippocampus (13). LTD triggered through metabotropic glutamate receptors relied on a direct binding of BRAG2 to the AMPAR subunit GluA2 (13).

Here, we studied a link among NMDAR activity, BRAG-mediated Arf6 activation, and synaptic maturation. Our results show that BRAG1 and BRAG2 are consecutively recruited by NMDARs during development and that a loss of BRAG1 or BRAG2 affects the number and strength of excitatory synapses.

Experimental Procedures

DNA Constructs—The cDNAs encoding fragments of the intracellular domains of GluN2A and GluN2B were inserted into pGEX-6P plasmids. Golgi-associated, γ-adaptin ear-containing, Arf-binding protein 3 (GGA3) fused to GST for Arf6$_{GTP}$-specific pulldown assays was expressed from pGEX-GGA3 (13). CMV expression constructs (23) for rat GluN1, rat GluN2A, and mouse GluN2B were kindly provided by Peter H. Seeburg. HA-tagged versions contain amino acids (aa) YPYD-VPDYA between aa 27 and 28 of immature GluN2A and between aa 28 and 29 of immature GluN2B. Mutations were introduced by overlap-extension PCR and sequenced by LGC Genomics. The cDNAs for rat BRAG1 (1154-amino acid isoform; aa 1–1151 of GenBank™ accession number NM_001277425 followed by aa VCY (GenBank accession number NM_001277386)) and rat BRAG2 (947-amino acid isoform; aa 1–933 of GenBank accession number NP_001127856 (*Mus musculus*) followed by aa FQPFQPSQPPVLCS) (13) were inserted into the CMV expression vector (23) in fusion with an N-terminal FLAG epitope. The rat cDNA for Arf6 was inserted into the CMV expression vector (23). HA-tagged Arf6 was expressed from pcDNA-Arf6-HA (13).

Viral Constructs—Double-stranded oligonucleotide adaptors for BRAG RNAi were first inserted into pCMV-U6 (24) and evaluated for knockdown efficiency and specificity in HEK293 cells. BRAG1-RNAi, BRAG2-RNAi, and BRAG-RNAi control (ctrl) encode the following short hairpin RNAs (5′–3′): GGA-AGCUAUCUAUCGGGAUAAGUGAAGCCACAGAUGUU-AUCCCGAUAGAUAGCUUCC (B1-RNAi), GCAUUGUGC-UGUCCAACAUGAGUGAAGCCACAGAUGUCAUGUUG-GACAGCACAAUGC (B2-RNAi) (13), and GCAGCUAAUG-GCCUUUCAUGAGUGAAGCCACAGAUGUCAUGAAAG-GCCAUUAGCUGC (ctrl-RNAi; scrambled version of B2-RNAi).

The U6-promoter-shRNA cassettes were then inserted into pFUGW, and lentivirus was produced, concentrated, and titered as described (13). For RNAi against both BRAG2 and BRAG1, the U6-promoter-shRNA cassettes were inserted in tandem (25). RNAi-mediated knockdown of endogenous BRAG1 and BRAG2 in neuronal cultures was evaluated by Western blotting (Figs. 4D and 5C). Cre expression vector FCKiGW (Flap, CaMKII promoter, internal ribosome entry site, GFP, WPRE)-Cre has been described before (13). Plasmids for lentiviral vectors (26) and RNAi (24) were provided by Dr. Carlos Lois and Dr. Pavel Osten.

Adeno-associated virus (AAV) constructs were generated by inserting NheI-BstBI fragments encompassing the U6-promoter-shRNA cassettes for BRAG1- and BRAG2-RNAi into pAAV-CAG-GFP (Addgene) equipped with an appropriate linker immediately upstream of the CAG-GFP cassette. Viral particles of AAV serotype 9 were produced by the Viral Core Facility of the Charité Berlin using an iodixanol gradient for purification (27) and quantitative PCR for quantification.

Antibodies—Antibodies to Arf6 (ab49931, Abcam), BRAG1 (sc-168198, Santa Cruz Biotechnology; HPA003973, Sigma-Aldrich), FLAG (F1804 and F7425, Sigma-Aldrich), GFP (ab13970, Abcam), GluA2 (MAB397, Millipore), GluN1 (11711, Synaptic Systems), GluN2A (07-632, Millipore), GluN2B (sc-9057, Santa Cruz Biotechnology), HA (HA.11, Covance), Homer1b/c (ab97593, Abcam), PSD-95 (MAB1596, Millipore), α-tubulin (T9026, Sigma-Aldrich), βIII-tubulin (TUJ1, Covance), and vesicular glutamate transporter 1 (VGLUT 1) (135304, Synaptic Systems) were purchased. The antibody to BRAG2 used for immunoblots was described previously (13). The antibody to BRAG2 used for immunocytochemistry (BRAG2 IC) was generated at BioGenes (Germany) by immunization of a rabbit with a bacterially expressed GST fusion protein containing a 187-amino acid fragment of murine BRAG2 (aa GPEK–RPEP). The resulting antiserum was first cleaned by incubation with a matrix containing GST fused to a 189-amino acid fragment of murine BRAG1 (aa EYEK–CRDF) and then affinity-purified on a matrix containing the protein used for immunization.

Cell Culture—Media and supplements were obtained from Life Technologies unless otherwise stated. Primary cortical neurons were prepared from rat embryos at embryonic day 18 (E18). Primary hippocampal neurons were prepared from E18 rat and E16.5 mouse embryos. Cortices and hippocampi were isolated in Hanks' balanced salt solution, dissociated with 1 mg/ml trypsin (Worthington), and triturated with fire-polished Pasteur pipettes. The cell suspension was washed twice in growth medium (Neurobasal® medium, B-27® serum-free supplement, penicillin (50 units/ml), streptomycin (50 μg/ml), 2 mM GlutaMAX) and plated on poly-DL-ornithine hydrobromide (Sigma-Aldrich)-coated plates or coverslips. Cortical neurons were plated at a density of 700,000 cells/well in 6-well plates and 350,000/per well in 12-well plates, whereas hippocampal neurons were plated on 12-mm coverslips placed in 24-well plates at 75,000 cells/well. Half of the medium was exchanged on day *in vitro* 2 (DIV2), DIV4, DIV9, and then once a week.

HEK293, HEK-BRAG1, and HEK-BRAG2 cells were maintained at 37 °C, 5% CO_2 in DMEM (4.5 mg/ml glucose, GlutaMAX™, pyruvate) supplemented with 10% FBS (Biochrom), 100 units/ml penicillin, and 100 μg/ml streptomycin. Medium

for HEK-BRAG1 and -BRAG2 cells was complemented with 150 μg/ml hygromycin. HEK-BRAG2 cells were plated on poly-L-lysine-coated dishes for transfections. HEK293FT cells used for lentivirus production were maintained at 37 °C, 5% CO_2 in DMEM (4.5 mg/ml glucose, L-glutamine), 10% FBS, 100 units/ml penicillin, 100 μg/ml streptomycin, 500 μg/ml geneticin, 1 mM sodium pyruvate, and non-essential amino acids. All cells were transfected using calcium phosphate precipitation and harvested 48–72 h after transfection. Cells transfected for NMDAR expression were kept in medium containing 50 μM $MgCl_2$ to prevent Ca^{2+}-mediated toxicity.

BRAG-expressing Cell Lines—An HEK293 cell line expressing a 1154-amino acid isoform of BRAG1 (HEK-BRAG1) was generated following the same protocol as for HEK-BRAG2 (13).

GST Pulldown Assay—GST fusion proteins were expressed in *Escherichia coli* BL21(DE3) (Stratagene) and purified on glutathione-Sepharose beads (GE Healthcare). For *in vitro* interaction studies, membrane-free extracts of transfected HEK293 cells (PBS, 1% Triton™ X-100, 1× Complete™ protease inhibitor mixture, pH 7.4) were precleared by incubation with a mixture of unloaded and GST-coupled glutathione beads and then incubated with beads coupled to the recombinant proteins for 2 h at 4 °C. Beads were washed in PBS containing 0.1% Triton X-100.

Arf6 Activity Measurements—To determine cellular Arf6 activities, an $Arf6_{GTP}$-specific pulldown assay (28) was used as described previously (13).

HEK293 cells were starved for 1 h in ECS (140 mM NaCl, 1.3 mM $CaCl_2$, 5.4 mM KCl, 25 mM HEPES, 33 mM glucose, pH 7.4) and then stimulated with 1 mM L-glutamate (Applichem) for 5 min in ECS. To test the importance of calcium influx, HEK293 cells were starved in ECS containing 1.3 mM $CaCl_2$ for 1 h, washed with ECS without $CaCl_2$, and then stimulated with 1 mM L-glutamate in ECS with or without 1.3 mM $CaCl_2$.

Primary cortical cultures were infected at DIV2 or DIV15. They were treated at DIV6–8 or DIV20–22 (referred to as DIV7 and DIV21 in the figures) with 100 μM D-AP5 (Tocris), 100 μM (+)-MK-801 maleate (Tocris), 3 μM ifenprodil (+)-tartrate salt (Sigma-Aldrich), 300 nM $ZnCl_2$ (Applichem), and/or 100 μM NMDA (Biotrend) in conditioned medium as indicated.

Arf6 activity was quantified by comparing background-corrected signal intensity densities of Arf6 pulldown (pd) and Arf6 total (t) bands on immunoblots. Band intensities were measured on the blot imager Fusion FX7 (Vilber Lourmat). Intensity values were obtained by Bio1D (Vilber Lourmat) and calculated with Microsoft Excel as pd/t ratios or effect percentages. GraphPad Prism version 5 for Windows was used for graphs and statistical analysis.

Results were expressed as means of active Arf6 ratios (pd/t) ±S.E. from at least three independent experiments and six independent values. In the case that test groups were compared in pairs of treated and untreated samples, activity ratios are shown as effect percentages compared with the untreated control. Statistical significance was evaluated by two-tailed unpaired or paired t tests as indicated. Differences were considered significant (*) at p values of less than 0.05.

Immunocytochemistry—HEK-BRAG1 and -BRAG2 cells were plated on poly-DL-ornithine hydrobromide-coated coverslips and transfected either for expression of Arf6-HA, GluN1, GluN2A, or GluN2B or for expression of Arf6, GluN1, and HA-GluN2A or HA-GluN2B. 24 h later, cells were fixed with 4% paraformaldehyde, permeabilized with 0.25% Triton X-100, blocked in 1% BSA, and incubated with primary antibodies overnight at 4 °C in 1% BSA. HEK-BRAG1 cells were stained with antibodies to BRAG1 (HPA003973; 1:100) and HA (1:1,000); HEK-BRAG2 cells were stained with antibodies to BRAG2 (IC; 1:500) and HA (1:1,000). Secondary Alexa Fluor fluorophore-conjugated antibodies were applied 1:1,000 for 1 h at room temperature, and the cells were mounted with Mowiol 4-88 (Sigma-Aldrich). Images of 0.4-μm-thick slices were taken on an SP8 confocal system (Leica Microsystems, Germany).

Hippocampal mouse or rat neurons were infected at DIV2 or DIV15. At DIV8 or DIV21–28, the cells were fixed with 4% paraformaldehyde, permeabilized with 0.25% Triton X-100, and blocked in 1% BSA. Primary antibodies to VGLUT 1 (1:1,000), PSD-95 (1:1,000), BRAG1 (HPA003973; 1:100), BRAG2 (IC; 1:500), GluN2A (1:200), GluN2B (1:200), Arf6 (1:100), Homer1b/c (1:1,000), and GFP (1:1,000) were applied overnight at 4 °C in 1% BSA. Secondary Alexa Fluor fluorophore-conjugated antibodies (1:1,000) were applied for 1 h at room temperature in 1% BSA and mounted with Mowiol. Images were taken on an SP8 confocal system. Maximal projections of Z-stacks were further analyzed in ImageJ. Synapse numbers and sizes were quantified as described (29).

Fluorescence Internalization Assay—Hippocampal rat neurons were infected at DIV15 and used at DIV24/25. Neurons were treated under live conditions at 37 °C, 5% CO_2 in their medium first for 10 min with mouse anti-GluA2 antibody (1:100). After three brief washings with conditioned medium, cells were stimulated with 100 μM NMDA for 3 min, washed once with medium, and incubated for an additional 7 min. Cells were then mildly fixed with 4% paraformaldehyde for 5 min, washed with PBS, blocked with 1% BSA for 30 min at room temperature, and incubated with Cy5-conjugated anti-mouse antibody (Jackson ImmunoResearch Laboratories; 1:500) in 1% BSA to visualize surface GluA2. After washing with PBS, cells were fixed and permeabilized with a 9:1 mixture of methanol and MES solution (100 mM MES (AppliChem), pH 6.9, 1 mM EDTA, 1 mM $MgCl_2$) for 90 s at −20 °C. Cells were again blocked for 30 min with 1% BSA, and chicken anti-GFP antibody (1:1,000) was applied for 1 h at room temperature. After washing with PBS, Cy3-conjugated anti-mouse antibody (Jackson ImmunoResearch Laboratories; 1:500) and Alexa Fluor 488-conjugated anti-chicken antibody (1:1,000) were applied for 1 h in 1% BSA. Coverslips were washed and mounted in Mowiol.

GFP-positive neurons were inspected on an SP5 confocal system (Leica Microsystems). The ratio of the mean intensities for Cy5 representing surface-remaining GluA2 and Cy3 representing intracellular GluA2 in segments of proximal dendrites was measured using ImageJ.

Animal Procedures—All animal procedures were in accordance with the "European Union's Directive 86/609/EEC" and

the Regional Boards in Berlin (G-0268/09, T-0269/11) and Karlsruhe (35-9185.81/G-273/12).

Electrophysiology in Berlin (Fig. 9)—Adeno-associated virus constructs expressing shRNA were injected unilaterally in the hippocampus of postnatal day 0 (P0) (BRAG1 RNAi or BRAG2 RNAi) and P21 (BRAG2 RNAi) mice. For viral injections in P0 mice, pups were briefly anesthetized with isoflurane. Viral constructs were directly injected in the hippocampal region at three different spots along the ventrodorsal axis 20 μm apart. The virus was pressure-injected using borosilicate glass capillaries (World Precision Instruments) pulled with a Zeitz DMZ Puller (Martinsried, Germany). For stereotaxic injections in P21 mice, animals were anesthetized with ketamine/xylazine (100 and 10 mg/kg, respectively). Hippocampal injections were done using the following coordinates (relative to bregma): medial/lateral, 3.60 mm; anterior/posterior, 3.28 mm; dorsal/ventral, 2.96 mm. Virus was injected at three spots 50 μm apart, 0.25 μl each using capillary micropipets (Drummond). At least 2 weeks after infection, mice were briefly anesthetized with isoflurane and decapitated. Brains were rapidly removed and transferred to cooled oxygenated artificial cerebrospinal fluid containing 87 mM NaCl, 26 mM NaHCO$_3$, 50 mM sucrose, 10 mM glucose, 2.5 mM KCl, 1.25 mM NaH$_2$PO$_4$, 3 mM MgCl$_2$, and 0.5 mM CaCl$_2$. Horizontal hippocampal slices (300 μm) were cut on a VT 1200 Vibratome (Leica Microsystems). Slices were then incubated at 34–35 °C in an interface-type storing chamber, and recordings were started after 1 h. All recordings were performed in artificial cerebrospinal fluid containing 119 mM NaCl, 26 mM NaHCO$_3$, 10 mM glucose, 2.5 mM KCl, 1 mM NaH$_2$PO$_4$, 1.3 mM MgCl$_2$, and 2.5 mM CaCl$_2$ at near-physiological temperature (~34 °C). All artificial cerebrospinal fluid solutions were equilibrated with 95% O$_2$ and 5% CO$_2$; osmolarity of artificial cerebrospinal fluid for recordings was maintained in the range of 290 and 305 mosM. Whole-cell patch clamp recordings were performed in a submerged recording chamber. For recordings, borosilicate glass electrodes (2–5 megaohms) were used filled with 130 mM KMeSO$_3$, 10 mM HEPES, 20 mM KCl, 4 mM NaCl, 4 mM Mg-ATP, 0.5 mM Na-GTP, and 5 mM sodium phosphocreatine; pH of the intracellular solution was adjusted to 7.2 with KOH. To isolate AMPAR miniature excitatory postsynaptic currents (mEPSCs), 1 μM SR 95531 (gabazine), 1 μM tetrodotoxin, 50 μM D-AP5, and 100 μM cyclothiazide were added to the extracellular recording solution. Principal cells located in the pyramidal cell layer of the hippocampal CA1 area were identified using infrared differential interference contrast video microscopy and adequate fluorescence filter settings visualizing GFP-tagged neurons. Series resistance (R_s) was monitored throughout experiments; cells were rejected if R_s was >20 megaohms. No R_s compensation was used. Collected signals were digitized with 16-bit resolution (National Instruments, Austin, TX) and sampled at 3 kHz using Igor Pro (Wavemetrics, Lake Oswego, OR). For mEPSC analysis, data were filtered to 1 kHz. For mEPSC collection, signals were first detected automatically using the Igor plug-in Neuromatics and in a second step manually sorted by visual inspection to exclude false positive events.

Electrophysiology in Mannheim (Fig. 10)—Surgeries of 3–4-week-old *Iqsec1$^{fl/fl}$* mice were carried out as described (13).

Viral stock of FCKiGW-Cre was injected into the left hippocampus using the following coordinates (relative to bregma): anterior/posterior, 2.6 and 2.9 mm; medial/lateral, 3.5 mm; and dorsal/ventral, 3.4–2.2 mm (every 300 μm about 130 nl). Acute transverse slices (280 μm) from the middle hippocampus were prepared at least 2 weeks after infection at 5–7 weeks of age and perfused, cut, and stored in a submerged chamber with sucrose saline (125 mM NaCl, 25 mM NaHCO$_3$, 2.5 mM KCl, 1.25 mM NaH$_2$PO$_4$, 7 mM MgSO$_4$, 0.5 mM CaCl$_2$, 10 mM glucose, and 65 mM sucrose bubbled with 95% O$_2$ and 5% CO$_2$; ~300 mosM).

EPSCs were evoked with biphasic electrical stimulation in stratum radiatum (~100–150 μm from stratum pyramidale and shifted toward subiculum). In whole-cell voltage clamp with C_{fast} and R_s compensated for, EPSCs were recorded at room temperature in a submerged chamber from green fluorescent CA1 pyramidal cells (EPC10, HEKA, Patchmaster software) in saline (125 mM NaCl, 25 mM NaHCO$_3$, 2.5 mM KCl, 1.25 mM NaH$_2$PO$_4$, 1 mM MgCl$_2$, 2 mM CaCl$_2$, 12.5 mM glucose, and 0.005 mM gabazine bubbled with 95% O$_2$ and 5% CO$_2$; ~300 mosM) with internal pipette solution (0.2 mM EGTA, 10 mM HEPES, ~125 mM cesium gluconate, 20 mM CsCl, 10 mM NaCl, 10 mM Na$_2$-phosphocreatine, 4 mM Mg-ATP, 0.3 mM Na$_3$-GTP, and 5 mM QX-314 chloride, pH 7.3; ~280 mosM). Control EPSCs were recorded from uninfected cells from the right hemisphere. AMPAR currents were recorded at −70 mV, and NMDAR currents were recorded at +40 mV after wash-in of 5 μM 2,3-dioxo-6-nitro-1,2,3,4-tetrahydrobenzo[*f*]quinoxaline-7-sulfonamide. Rise of NMDAR currents was determined by the slope of a 20–80% linear fit normalized to the respective amplitude, decay of NMDAR current by a monoexponential fit, and paired pulse ratios with an interstimulus interval of 50 ms. The coefficient of variation (CV) was the ratio of standard deviation and average EPSC amplitude per cell (15–30 repetitions per cell). Mean EPSC was plotted against inverse squared CV (CV^{-2}) assuming that (i) CV^{-2} = $n \times P_r/(1 - P_r)$ with a constant average release probability of P_r = 0.3 (30) and (ii) mean EPSC is proportional to the number n of stimulated synapses and to the number of actually releasing synapses, which we call n_r ($n_r = n \times P_r$). Therefore, quantal size q is proportional to the slope of a linear fit through the origin, *i.e.* q = slope/(1 - P_r) because CV^{-2} = $n_r/(1 - P_r)$ and mean EPSC = $q \times n_r$.

Statistical significances (*, $p < 0.05$) were assessed in GraphPad Prism 5.02 or Igor Pro 6.36 (Wavemetrics) via t test if not indicated otherwise.

Results

NMDARs Stimulate BRAG1 and BRAG2 in a Subtype-selective Manner in HEK293 Cells—To assess potential signaling from NMDARs to BRAGs, we co-expressed diheteromeric NMDARs consisting of GluN1 and either GluN2A or GluN2B and BRAG1 or BRAG2 in HEK293 cells and measured changes in Arf6 activity following stimulation with glutamate (Fig. 1*A*). GluN2B-containing NMDARs triggered an increase in the Arf6-GTP level through BRAG1. Vice versa, activation of GluN2A-containing NMDARs increased the Arf6 activity upon co-expression with BRAG2. In contrast, in cells expressing GluN2B and BRAG2 or GluN2A and BRAG1, the Arf6 activity
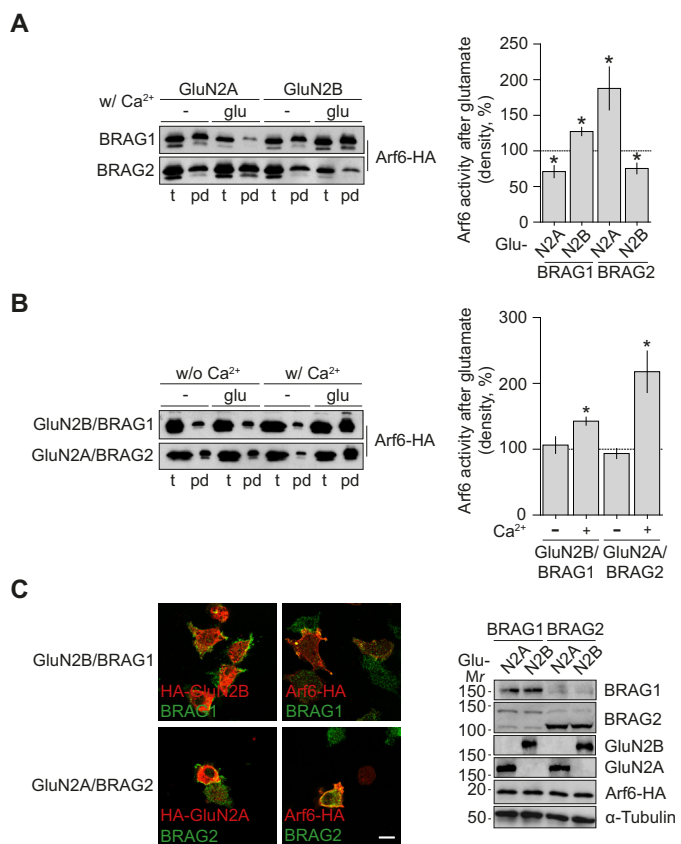
FIGURE 1. **Ligand binding to NMDARs stimulates BRAG-mediated Arf6 activation in a subtype-selective and Ca²⁺-dependent manner.** *A*, subtype-selective stimulation of BRAG1 and BRAG2 by ligand binding to NMDARs in HEK293 cells. Shown are representative immunoblots of Arf6$_{GTP}$-specific pulldown assays from HEK-BRAG1 and HEK-BRAG2 cells expressing Arf6-HA, GluN1, and either GluN2A or GluN2B. *Bars* illustrate Arf6 activation calculated as the Arf6$_{GTP}$/Arf6$_{total}$ ratio (pd/t) of cells treated for 5 min with 1 mM L-glutamate (*glu*) normalized to untreated controls (paired *t* test: HEK-BRAG1: GluN2A, *, $p = 0.0099$, $n = 9$; GluN2B, *, $p = 0.0033$, $n = 7$; HEK-BRAG2: GluN2A, *, $p = 0.043$, $n = 6$; GluN2B, *, $p = 0.025$, $n = 6$). *B*, NMDAR-BRAG signaling requires Ca²⁺. Shown are representative immunoblots of Arf6$_{GTP}$-specific pulldown assays from HEK-BRAG1 cells expressing Arf6-HA, GluN1, and GluN2B and from HEK-BRAG2 cells expressing Arf6-HA, GluN1, and GluN2A. Cells were stimulated by application of an extracellular solution containing L-glutamate (*glu*) with or without 1.3 mM Ca²⁺. *Bars* illustrate Arf6 activation calculated as the Arf6$_{GTP}$/Arf6$_{total}$ ratio (pd/t) of cells treated with glutamate in the presence or absence of extracellular Ca²⁺ normalized to untreated controls (paired *t* test: HEK-BRAG1: without (*w/o*) Ca²⁺, *, $p = 0.63$, $n = 11$; with Ca²⁺, *, $p = 0.0009$, $n = 6$; HEK-BRAG2: without Ca²⁺, $p = 0.88$, $n = 8$; with Ca²⁺, *, $p = 0.010$, $n = 6$). *Error bars* indicate S.E. *C*, subcellular distribution and expression levels of NMDARs, BRAGs, and Arf6 in transfected HEK-BRAG1 and -BRAG2 cells. NMDARs with HA-tagged GluN2 subunits and untagged Arf6 were expressed to compare the localization of GluN2B and BRAG1 or GluN2A and BRAG2 (*left column*). NMDARs with untagged GluN2 subunits and Arf6-HA (*right column*, as in *A* and *B*) were expressed to compare the localization of BRAG1 or BRAG2 and Arf6. The distribution of the stained proteins was similar upon expression of GluN2A in HEK-BRAG1 and GluN2B in HEK-BRAG2 cells (not shown). Western blots show the expression levels of GluN2 subunits, BRAGs, and Arf6-HA in homogenates of HEK-BRAG1 and HEK-BRAG2 cells transfected as in *A* and *B*. *Scale bar*, 10 μm.

was decreased by the glutamate treatment. Omission of calcium from the extracellular solution during stimulation prevented glutamate-triggered Arf6 activation, indicating that NMDAR-BRAG signaling requires calcium influx (Fig. 1*B*). BRAG1, BRAG2, and Arf6 were enriched at sites close to the plasma membrane in line with their regulation by surface-expressed NMDARs (Fig. 1*C*). Thus, it appears that the
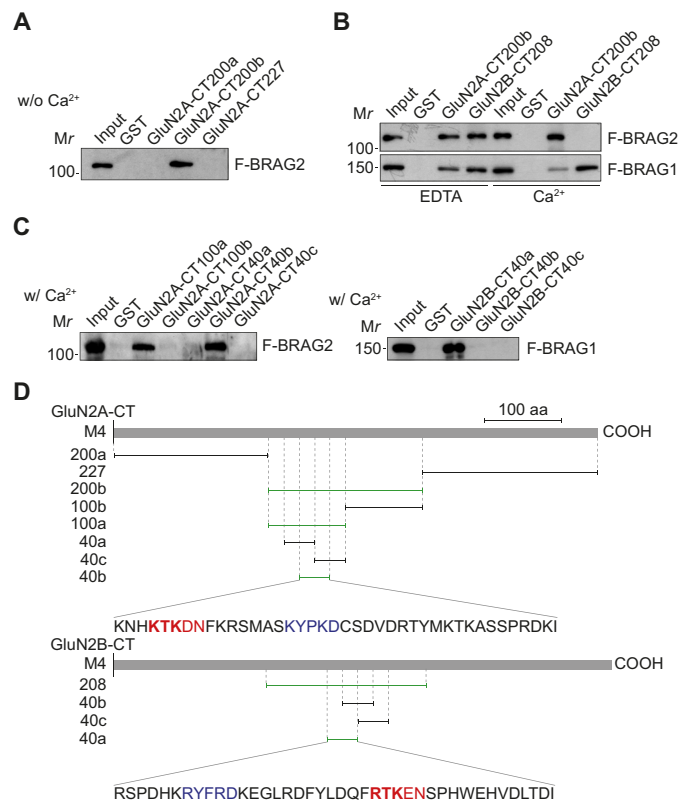

FIGURE 2. **Physical interaction between NMDARs and BRAG proteins.** *A*, the central part of the intracellular domain of GluN2A binds to BRAG2. An immunoblot of recombinant FLAG (*F*)-tagged BRAG2 pulled down from a HEK293 cell extract by GST fused to aa 838–1037 (GluN2A-CT200a), aa 1038–1237 (GluN2A-CT200b), and aa 1238–1464 (GluN2A-CT227) of GluN2A in the presence of 2 mM EDTA is shown. GluN2A-CT200a was recovered from inclusion bodies (50). Input, 5% of cell extract. *B*, Ca²⁺ promotes selective interactions between GluN2 fragments and BRAGs. Immunoblots of recombinant FLAG-tagged BRAG2 or BRAG1 recovered from HEK293 cell extracts by GST fused to aa 1036–1243 of GluN2B (GluN2B-CT208) in the presence of 2 mM EDTA or 100 μM Ca²⁺ are shown. Input, 5% of cell extract. *C*, BRAGs interact with short regions in GluN2 subunits. Immunoblots of recombinant FLAG-tagged BRAG proteins recovered from HEK293 cell extracts by GST pulldown with 40- or 100-amino acid fragments of GluN2A (GluN2A-CT100a, aa 1038–1137; GluN2A-CT100b, aa 1138–1237; GluN2A-CT40a, aa 1058–1097; GluN2A-CT40b, aa 1078–1117; GluN2A-CT40c, aa 1098–1137) and GluN2B (GluN2B-CT40a, aa 1115–1154; GluN2B-CT40b, aa 1135–1174; GluN2B-CT40c, aa 1155–1194) in the presence of 2 mM Ca²⁺. Input, 5% of cell extract. *D*, interaction sites for BRAG2 and BRAG1 within GluN2 intracellular C-terminal tails. The scheme indicates the location of the protein fragments used for the interaction analyses within the C-terminal regions of GluN2A and GluN2B. NMDAR fragments shown to interact with BRAG1 or BRAG2 are depicted in *green*. Sequences of the shortest interacting fragments in single letter code of amino acids are shown below with conserved motifs in *red* and *blue*. Importance of the KTK/RTK motif (*bold*) was tested in Fig. 3.

closely related Arf6 GEFs BRAG1 and BRAG2 are able to mediate calcium-dependent, subtype-specific functions of the NMDAR.

NMDAR-BRAG Signaling Depends on Binding Sites in the GluN2 C-terminal Tails—We used GST pulldown assays to test for interactions between the intracellular domains of GluN2 subunits and BRAGs (Fig. 2). A 200-amino acid region centrally located within the intracellular domain of GluN2A bound BRAG2 (Fig. 2*A*). In a calcium-free buffer, this fragment of GluN2A as well as the corresponding region of GluN2B pulled down both BRAGs without preference. In contrast, in the presence of 100 μM Ca²⁺, GluN2A pulled down less BRAG1 than
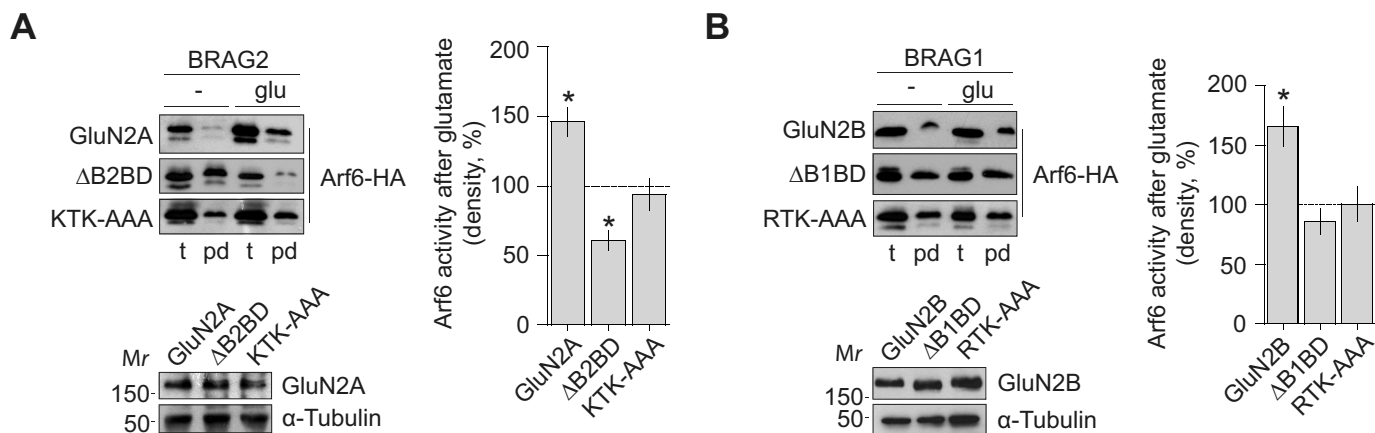
FIGURE 3. **NMDAR-BRAG signaling requires physical interaction.** *A* and *B*, BRAG recruitment upon ligand binding to NMDARs depends on a physical interaction. Shown are results of Arf6$_{GTP}$-specific pulldown assays from HEK-BRAG1 and HEK-BRAG2 cells expressing Arf6-HA, GluN1, and GluN2A (*A*) or GluN2B (*B*) with or without the indicated deletions or mutations. $\Delta B2BD$, deletion of BRAG2-binding domain in GluN2A (aa 1078–1117; GluN2A-CT40b in Fig. 2*C*); *KTK-AAA*, mutation K1081A/T1082A/K1083A in GluN2A; $\Delta B1BD$, deletion of BRAG1-binding domain in GluN2B (aa 1115–1154; GluN2B-CT40a in Fig. 2*C*); *RTK-AAA*, mutation R1138A/T1139A/K1140A in GluN2B. Western blots on the *bottom* indicate that the mutations did not affect the expression levels of GluN2A or GluN2B. *Bars* illustrate Arf6 activation calculated as the Arf6$_{GTP}$/Arf6$_{total}$ ratio (pd/t) of cells treated with 1 mM glutamate for 5 min normalized to untreated controls (paired *t* test: *A*, HEK-BRAG2: GluN2A, *, $p = 0.0012$, $n = 14$; $\Delta B2BD$, *, $p = 0.030$, $n = 7$; $\Delta 260$, *, $p = 0.017$, $n = 6$; K1081A/T1082A/K1083A, $p = 0.075$, $n = 9$; *B*, HEK-BRAG1: GluN2B, *, $p = 0.0007$, $n = 14$; $\Delta B1BD$, $p = 0.14$, $n = 8$; R1138A/T1139A/K1140, $p = 0.14$, $n = 10$). *Error bars* indicate S.E. *Left*, representative immunoblots.

GluN2B, whereas BRAG2 was pulled down exclusively by GluN2A (Fig. 2*B*). This finding suggests that calcium has an impact on the interaction between NMDARs and BRAG proteins. Further mapping of the BRAG binding sites within GluN2A and GluN2B revealed 40-amino acid fragments able to interact with BRAGs in the GST pulldown assay (Fig. 2, *C* and *D*). Glutamate stimulation of NMDARs lacking these regions either decreased the Arf6 activity (Fig. 3*A*) or had no effect on the Arf6-GTP level (Fig. 3*B*) in contrast to full-length receptors. These data indicate that both a rise in the calcium concentration and interaction sites in the cytoplasmic region of the GluN2 subunits are required for the activation of BRAG1 and BRAG2.

A comparison of the GluN2 sequences interacting with BRAG1 and BRAG2 revealed two short stretches of conserved amino acids (Fig. 2*D*). Interestingly, they are present in the opposite order in GluN2A and GluN2B. Mutation of **KTK**DN to **AAA**DN in GluN2A and **RTK**EN to **AAA**EN in GluN2B prevented the glutamate-triggered Arf6 activation through NMDARs and BRAGs in HEK293 cells (Fig. 3, *A* and *B*). This result suggests that the amino acids ^{1081}KTK^{1083}/^{1138}RTK^{1140} in GluN2A/2B are required for signal transduction from NMDARs to BRAGs.

BRAGs Mediate NMDAR-driven Arf6 Activation in Neuronal Cultures—It is well established that NMDARs are restricted to GluN2B or GluN2D in terms of GluN2 subunit expression at embryonic stages, whereas during postnatal development the contribution of GluN2A is continuously increasing (3–5). We therefore chose to analyze NMDAR effects on endogenous Arf6 in primary cortical neuron cultures at a young (DIV6–8) and at a mature (DIV20–22) stage. The expression levels of BRAG1, BRAG2, and GluN2A were much higher in mature than in young neurons, whereas GluN2B and Arf6 showed only minor changes (Fig. 9*D*). In young cultures, we found the Arf6 activity to be significantly higher than in mature cultures (Fig. 4*A*). The Arf6 activity of young neurons was decreased by both the

NMDAR antagonist D-AP5 (Fig. 4*A*) and the NMDAR channel blocker MK-801 (Fig. 4*B*), suggesting an endogenous stimulatory NMDAR activity on Arf6 at this stage. We tried to isolate subtype-selective effects using 3 μM ifenprodil to prevent activation of heterodimeric GluN1/GluN2B NMDARs or 300 nM Zn^{2+}, which blocks preferentially GluN2A-containing NMDARs at this concentration (31–34). The endogenous NMDAR signaling on Arf6 in young neurons was blocked by 3 μM ifenprodil but not by 300 nM Zn^{2+}, suggesting it was mediated by GluN2B (Fig. 4*B*). Next, we infected neurons at DIV2 with lentiviral vectors expressing short hairpin RNAs to deplete BRAG1 or BRAG2. Ifenprodil reduced the Arf6 activity in control (scrambled shRNA)- and BRAG2-RNAi-infected but not in BRAG1-RNAi-infected neurons at DIV7 (Fig. 4, *C* and *D*). In the absence of BRAG1, ifenprodil actually increased the Arf6 activity, suggesting a negative tone of GluN2B on Arf6 under these conditions. These data indicate that BRAG1 is mediating endogenous GluN2B-dependent signaling on Arf6 in young neuronal cultures.

In mature neurons, application of D-AP5 did not decrease the Arf6-GTP level (Fig. 4*A*), but stimulation with NMDA for 5 min caused an activation of Arf6 that was blocked by D-AP5 or MK-801 (Fig. 5*A*). The NMDA-triggered Arf6 activation in mature neuronal cultures was not affected by 3 μM ifenprodil, indicating that it was not mediated by GluN1/GluN2B receptors and that it might be caused by NMDARs containing GluN2A. Indeed, the NMDA stimulus did not lead to an activation of Arf6 in the presence of 300 nM Zn^{2+}. Next, we infected neurons at DIV15 to deplete BRAG1 or BRAG2 in mature neurons and found that NMDA-triggered activation of Arf6 at DIV21 specifically relied on BRAG2 (Fig. 5, *B* and *C*). In the absence of BRAG2, NMDA caused a drop in Arf6 activity. Thus, in line with our experiments in HEK293 cells, NMDARs containing GluN2A signal through BRAG2. In summary, during the development of cortical neurons in culture, the two major NMDAR subtypes of the
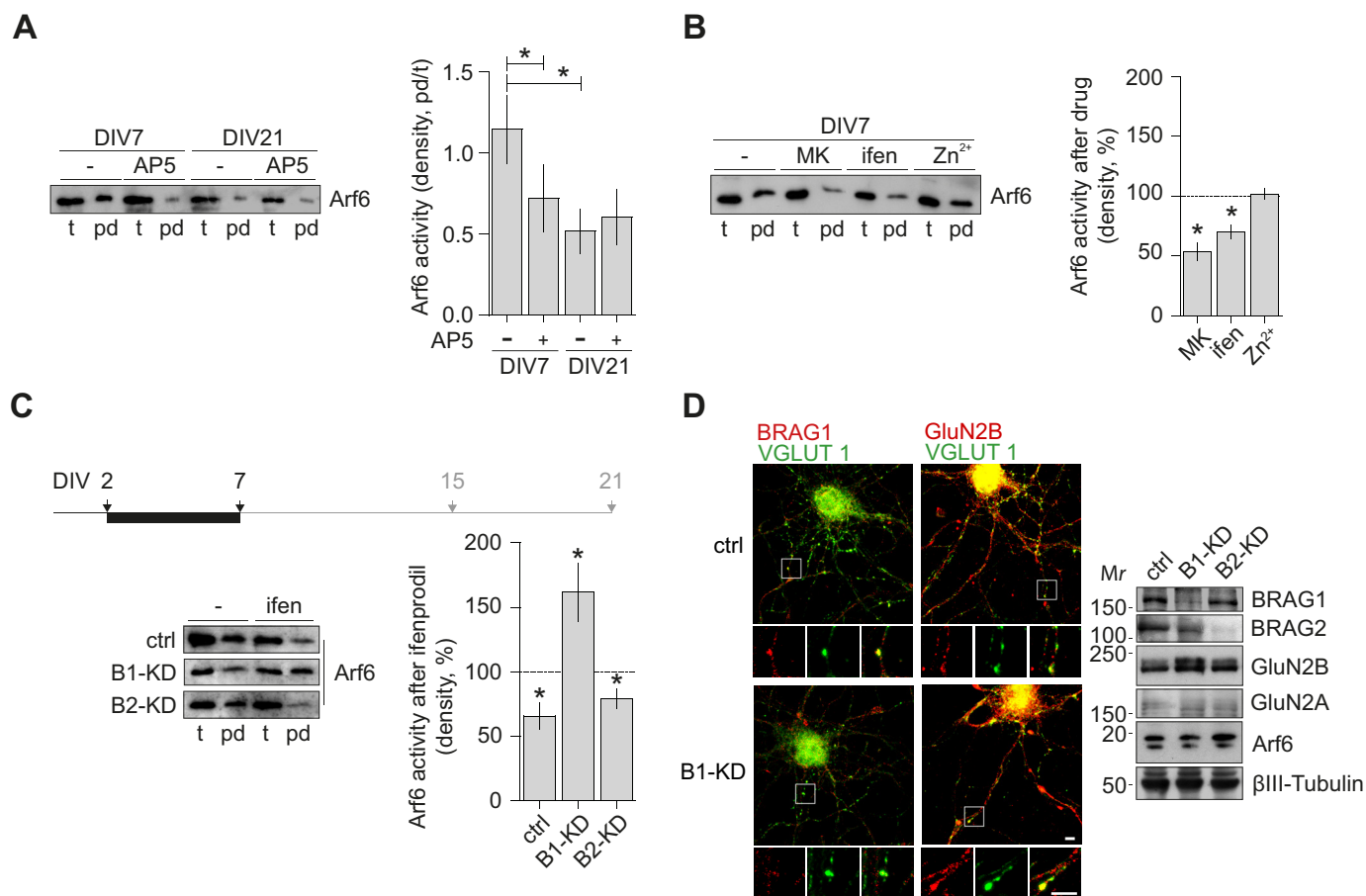
FIGURE 4. **Tonic Arf6 activation through GluN2B-BRAG1 signaling in young neurons.** *A*, differences in Arf6 activity between immature and mature cortical neuron cultures. Shown are results of Arf6$_{GTP}$-specific pulldown assays from cultured cortical neurons at DIV7 and DIV21 ($\pm$1 day for each) treated with or without 100 μM D-AP5 (*AP5*) for 1 h (paired *t* test: DIV7, *, $p < 0.0001$, $n = 8$; DIV21, $p = 0.057$, $n = 6$; unpaired *t* test: basal DIV7 *versus* DIV21, *, $p = 0.038$, $n = 6–8$). Levels of Arf6 activity are shown as Arf6$_{GTP}$/Arf6$_{total}$ ratios (pd/t). *B*, tonic Arf6 activation in immature neuronal cultures depends on GluN2B. Shown are results of Arf6$_{GTP}$-specific pulldown assays from cultured cortical neurons at DIV7 treated for 1 h with 100 μM MK-801 (*MK*), 3 μM ifenprodil (*ifen*), or 300 nM Zn^{2+}. Changes in Arf6 activity by drugs were calculated as the Arf6$_{GTP}$/Arf6$_{total}$ ratio (pd/t) normalized to an untreated control (paired *t* test, MK-801, *, $p = 0.0054$, $n = 7$; ifenprodil, *, $p = 0.0005$, $n = 8$; Zn^{2+}, $p = 0.83$, $n = 6$). *C*, tonic Arf6 activation through GluN2B in young cortical cultures is mediated by BRAG1. Cultured cortical neurons (DIV7) infected with lentiviral vectors delivering shRNAs to BRAG1 (*B1-KD*), BRAG2 (*B2-KD*), or a scrambled control hairpin (*ctrl*) at DIV2 were treated with or without 3 μM ifenprodil for 1 h. Changes in Arf6 activity were calculated as the Arf6$_{GTP}$/Arf6$_{total}$ ratio (pd/t) normalized to the respective control without ifenprodil (paired *t* test: ctrl, *, $p = 0.021$, $n = 9$; BRAG1-KD, *, $p = 0.031$, $n = 11$; BRAG2-KD, *, $p = 0.007$, $n = 10$). *Top*, timeline of neurons in culture indicating times of infection and experiment (*black arrows*). *Error bars* indicate S.E. *Left*, representative immunoblots. *D*, the distribution and expression level of GluN2B were not affected by BRAG1 depletion in young neuronal cultures. *Left*, at DIV8, BRAG1 co-localized with the synaptic marker VGLUT 1 in mouse hippocampal neurons. A subset of GluN2B co-localized with VGLUT 1 in neurons infected with a control virus as well as in neurons infected for BRAG1 RNAi at DIV2. *Right*, immunoblots of cell homogenates indicated that the expression levels of GluN2B, GluN2A, and Arf6 were not altered by depletion of BRAG1 or BRAG2 in young rat cortical cultures. *Scale bars*, 5 μm.

forebrain lacking or containing GluN2A triggered GDP/GTP exchange on Arf6 through BRAG1 or BRAG2, respectively.

Surprisingly, mature neurons infected for BRAG2 RNAi at DIV15 displayed an increased basal activity of Arf6 that was sensitive to ifenprodil in contrast to control-infected neurons (Fig. 6*A*). Thus, the knockdown of BRAG2 in mature neurons resulted in GluN2B-mediated Arf6 activation reminiscent of the situation in young neurons (Fig. 4*B*). To check whether the ifenprodil-sensitive Arf6 activity depended on BRAG1, we infected neurons with a vector for RNAi against both BRAG1 and BRAG2 at DIV15. Although this approach was less efficient in reducing the expression of BRAG1 and BRAG2 as compared with the respective single knockdowns (Fig. 4*C*), it entirely blocked NMDA-triggered Arf6 activation in mature neurons (Fig. 5*B*). Neurons carrying the knockdown construct for both BRAGs had a low Arf6 activity that was not

sensitive to ifenprodil, suggesting that BRAG1 mediates GluN2B-triggered Arf6 activation in mature neurons lacking BRAG2 (Fig. 6*A*). Treatment of mature cultures with 300 nM Zn^{2+} had a similar effect as the knockdown of BRAG2: an increased basal ifenprodil-sensitive Arf6 activity that was prevented by a knockdown of BRAG1 applied at DIV15 (Fig. 6*B*). These data imply that an interference with the GluN2A-BRAG2 pathway in mature synapses reinstalls GluN2B-BRAG1 signaling.

Together, our Arf6 activity measurements suggest that BRAG1 mediates tonic GluN2B-triggered Arf6 activation in young neurons in culture, whereas in mature neurons BRAG2 mediates GluN2A-triggered Arf6 activation upon NMDAR stimulation. This developmental shift appears to be reversible as depletion of BRAG2 or GluN2A blockade in mature neurons resulted in a high Arf6 activity mediated by GluN2B and BRAG1.
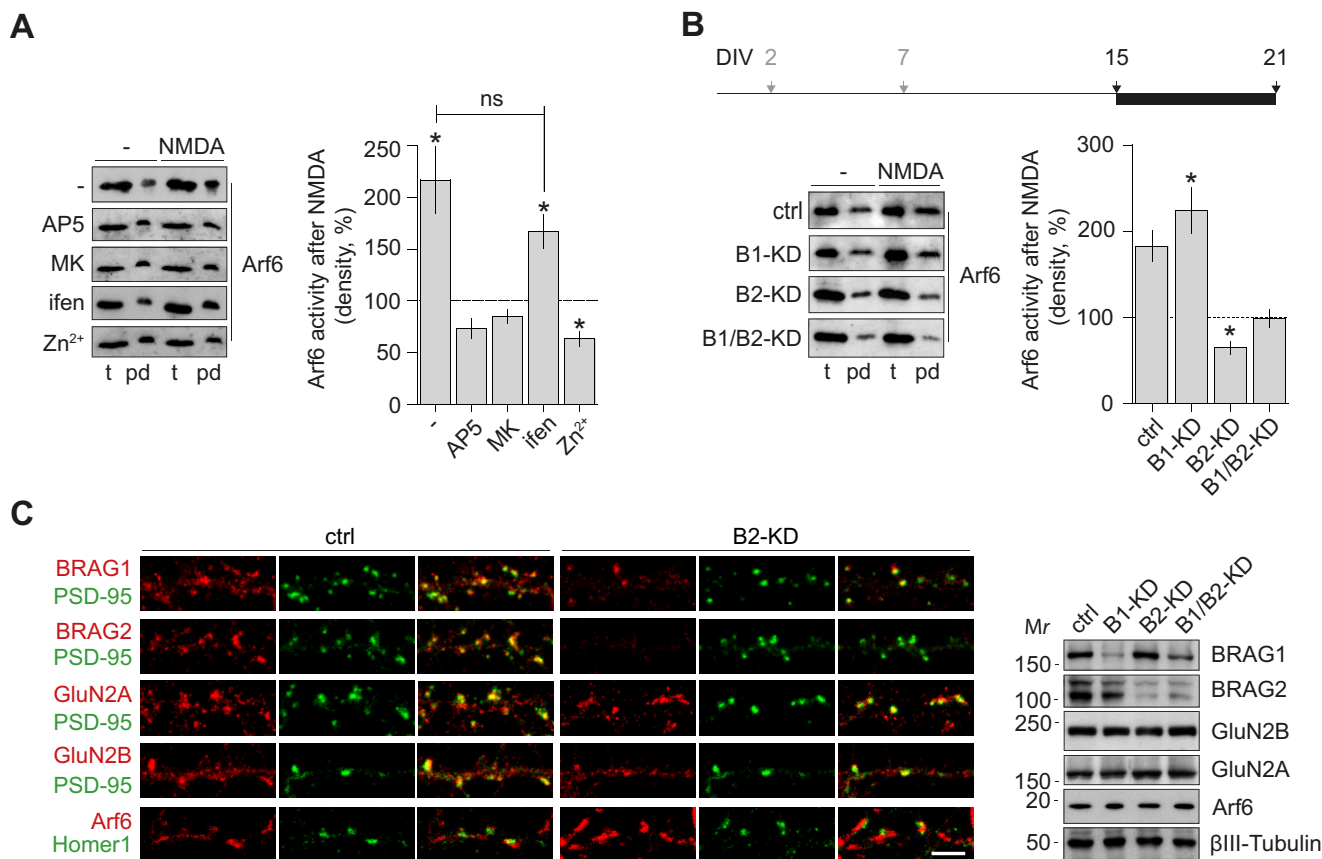
FIGURE 5. **NMDA-triggered Arf6 activation through GluN2A-BRAG2 signaling in mature neurons.** *A*, NMDA-triggered Arf6 activity in mature cortical cultures depends on GluN2A. Shown are results of Arf6$_{GTP}$-specific pulldown assays from cultured cortical neurons at DIV21 stimulated by 100 μM NMDA for 5 min in the presence or absence of 100 μM D-AP5 (*AP5*), 100 μM MK-801 (*MK*), 3 μM ifenprodil (*ifen*), or 300 nM Zn^{2+}. Arf6 activation by NMDA was calculated as the Arf6$_{GTP}$/Arf6$_{total}$ ratio (pd/t) normalized to the respective control without NMDA (paired *t* test: $-$, *, $p = 0.0007$, $n = 15$; D-AP5, $p = 0.059$, $n = 9$; MK-801, $p = 0.058$, $n = 10$; ifenprodil, *, $p = 0.0016$, $n = 10$; Zn^{2+}, *, $p = 0.0049$, $n = 10$). The NMDA-triggered Arf6 activation was not altered by ifenprodil (unpaired *t* test: $p = 0.24$, $n = 10-15$). *ns*, not significant. *B*, NMDA-triggered Arf6 activation in mature cortical cultures is mediated by BRAG2. Cultured cortical neurons (DIV21) infected at DIV15 with lentiviral vectors delivering shRNAs to BRAG1 (*B1-KD*), BRAG2 (*B2-KD*), or a control hairpin (*ctrl*) were treated with or without 100 μM NMDA for 5 min. Arf6 activation was calculated as the Arf6$_{GTP}$/Arf6$_{total}$ ratio (pd/t) normalized to the respective control without NMDA (paired *t* test: ctrl, *, $p = 0.0021$, $n = 17$; BRAG1-KD, *, $p = 0.012$, $n = 8$; BRAG2-KD, *, $p = 0.044$, $n = 12$; BRAG1/2-KD, $p = 0.35$, $n = 9$). *Top*, timeline of neurons in culture indicating times of infection and experiment (*black arrows*). *Error bars* indicate S.E. *Left*, representative immunoblots. *C*, synaptic localization and expression levels of the proteins involved in NMDAR-Arf6 signaling. *Left*, BRAG1, BRAG2, GluN2A, and GluN2B partly co-localized with the synaptic marker PSD-95 in mouse hippocampal neuron cultures at DIV21. Arf6 was broadly distributed in dendritic shafts, and a subset co-localized with Homer1. These patterns were not changed by the knockdown of BRAG2 (*B2-KD*). *Right*, immunoblots of cell homogenates indicated that the levels of the GluN2 subunits and Arf6 were not altered by knockdown of BRAG1 (*B1-KD*), BRAG2 (*B2-KD*), or both (*B1/2-KD*) in mature rat cortical cultures. *Scale bar*, 5 μm.
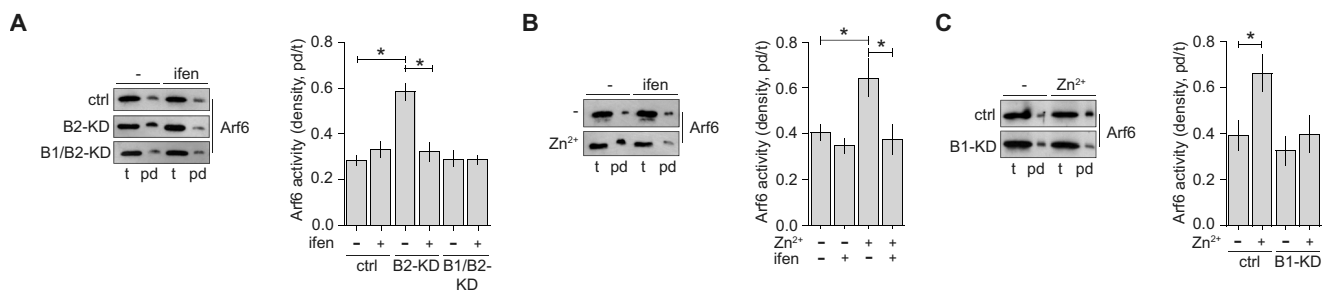

FIGURE 6. **Upon BRAG2 knockdown or GluN2A blockade, neurons revert to tonic Arf6 activation through GluN2B-BRAG1 signaling.** *A*, tonic Arf6 activation by GluN2B and BRAG1 in mature cortical cultures upon depletion of BRAG2. Cultured cortical neurons (DIV21) infected at DIV15 with lentiviral vectors delivering shRNAs to BRAG2 (*B2-KD*), to both BRAG1 and BRAG2 (*B1/2-KD*), or a scrambled control hairpin (*ctrl*) were treated with or without 3 μM ifenprodil (*ifen*) for 1 h (paired *t* test: ctrl, $p = 0.20$, $n = 10$; BRAG2-KD, *, $p < 0.0001$, $n = 12$; BRAG1/2-KD, $p = 0.89$, $n = 6$; unpaired *t* test: BRAG2-KD $-$ *versus* ctrl $-$, *, $p < 0.0001$, $n = 10-13$; BRAG1/2-KD $-$ *versus* ctrl $-$, $p = 0.86$, $n = 6-10$). Levels of Arf6 activity are shown as Arf6$_{GTP}$/Arf6$_{total}$ ratios (pd/t). *B* and *C*, tonic Arf6 activation by GluN2B and BRAG1 in mature cortical cultures upon Zn^{2+} treatment. *B*, cultured cortical neurons (DIV21) were treated with or without 300 nM Zn^{2+} for 1 h and subsequently with or without 3 μM ifenprodil for an additional hour (unpaired *t* test: Zn^{2+} effect, *, $p = 0.016$, $n = 10$; paired *t* test: ifenprodil effect without prior Zn^{2+} treatment, $p = 0.63$, $n = 6$; ifenprodil effect after Zn^{2+} treatment, *, $p < 0.0001$, $n = 10$). *C*, mature neuronal cultures (DIV21) infected at DIV15 with lentiviral vectors delivering an shRNA to BRAG1 (*B1-KD*) or a scrambled control hairpin (*ctrl*) were treated with or without 300 nM Zn^{2+} for 1 h (paired *t* test: ctrl, *, $p = 0.0015$, $n = 9$; BRAG1-KD, $p = 0.56$, $n = 8$; unpaired *t* test: knock-down effect, $p = 0.49$, $n = 8-9$). Levels of Arf6 activity are shown as Arf6$_{GTP}$/Arf6$_{total}$ ratios (pd/t). *Error bars* indicate S.E. *Left*, representative immunoblots.

Effects of BRAG1 and BRAG2 Depletion on the Number and Size of Glutamatergic Synapses in Primary Neuronal Cultures—We examined synapses in mature neuronal cultures by co-staining the presynaptic marker VGLUT 1 and the postsynaptic marker PSD-95. The knockdown of either BRAG1 or BRAG2 reduced the number of overlapping puncta by about 20%. However, the knockdown of BRAG2 diminished the average total size of the overlapping puncta, whereas the knockdown of BRAG1 did not affect the size of synaptic contacts (Fig. 7). The reduced synapse size may be related to the increased Arf6 activity that occurred upon knockdown of BRAG2 but not upon knockdown of BRAG1 in mature neuronal cultures (Fig. 6, *A* and *C*).

Effects of BRAG1 and BRAG2 Depletion on NMDA-triggered AMPA Receptor Internalization in Primary Neuronal Cultures—NMDARs control AMPAR trafficking to fine-tune synaptic transmission. We asked whether BRAG1 or BRAG2 was involved in NMDA-triggered internalization of the principal AMPAR subunit GluA2 in dendritic segments of mature hippocampal neurons in culture (Fig. 8). NMDAR stimulation increased GluA2 internalization in control-infected neurons. RNAi-mediated knockdown of BRAG2, but not of BRAG1, interfered with this effect. However, in neurons lacking BRAG2, GluA2 internalization prior to stimulation was higher than in control-infected neurons, potentially occluding the NMDA effect. As the knockdown of BRAG2 in mature cortical cultures resulted in an increased Arf6 activity (Fig. 6*A*) and precluded NMDA-triggered Arf6 activation (Fig. 5*C*), these data are consistent with a role of BRAG2-mediated Arf6 activation in NMDA-triggered GluA2 internalization in mature neurons.

Effects of BRAG1 and BRAG2 Depletion on Spontaneous AMPAR mEPSCs in Hippocampal CA1 Pyramidal Neurons—To analyze the effects of BRAG1 and BRAG2 on functional synapses during development, we injected adeno-associated virus constructs expressing the shRNAs targeting BRAG1 or BRAG2 into the hippocampal region of mice shortly after birth. Spontaneous AMPAR mEPSCs were recorded from infected (BRAG1 knockdown (KD) and BRAG2-KD) and uninfected (ctrl) CA1 pyramidal neurons around P16. Whereas BRAG2 depletion did not affect mEPSC frequency or amplitude in this setting (Fig. 9*B*; ctrl, $n = 7$ *versus* BRAG2-KD, $n = 9$; frequency, $p = 0.88$; amplitude, $p = 0.70$), knockdown of BRAG1 decreased the frequency but not the average amplitude (Fig. 9*A*; ctrl, $n = 12$ *versus* BRAG1-KD, $n = 14$; frequency, $p = 0.048$; amplitude, $p = 0.23$).

To test whether BRAG2 signaling exerts its impact in adult animals, we injected the viral construct for BRAG2 RNAi at P21 and recorded mEPSCs starting at P35. Now BRAG2 knockdown significantly reduced the frequency of synaptic events to levels seen in P16 neurons but did not alter their average amplitude (Fig. 9*C*; ctrl, $n = 7$ *versus* BRAG2-KD, $n = 8$; frequency, $p = 0.003$; amplitude, $p = 0.92$).

The hippocampal expression levels of BRAG1, BRAG2, and GluN2A but not of GluN2B and Arf6 increased between P14 and P36, although the differences were smaller than in rat cortical cultures between DIV8 and DIV22 (Fig. 9*D*). In addition,
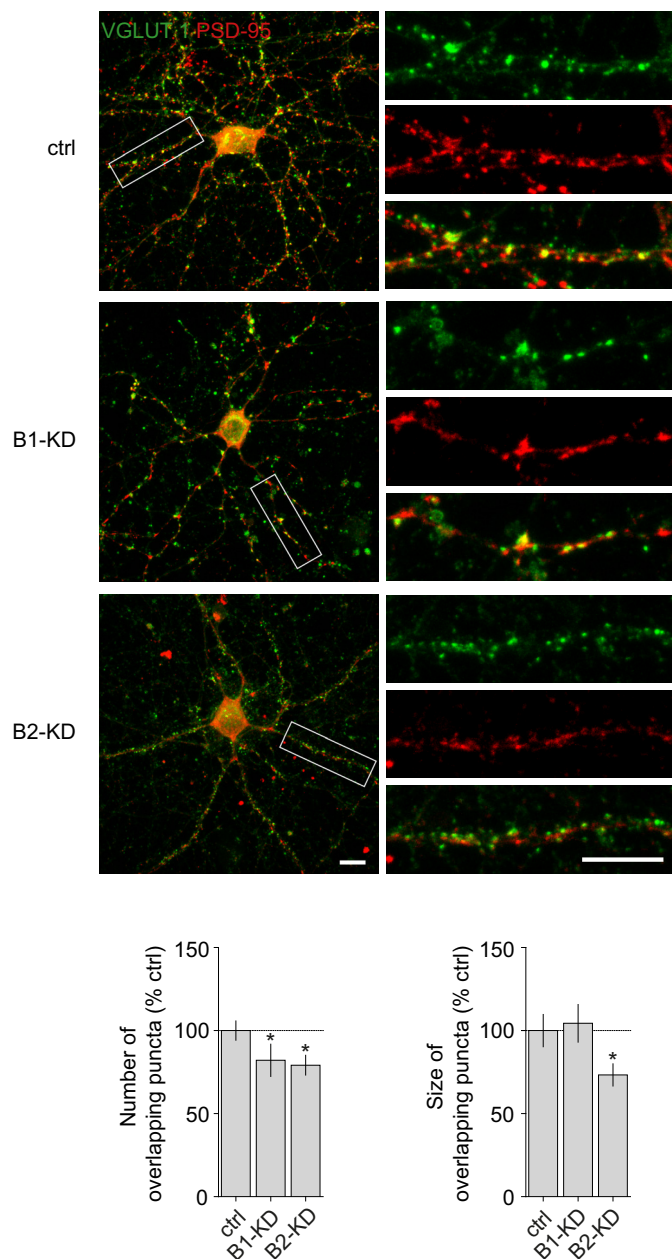

FIGURE 7. **Effects of the knockdown of BRAG1 and BRAG2 on the number and size of glutamatergic synapses.** VGLUT 1 and PSD-95 were stained in mature rat hippocampal neurons (DIV21–28) infected at DIV15 with lentiviral vectors delivering shRNAs to BRAG1 (*B1-KD*), BRAG2 (*B2-KD*), or a control hairpin (*ctrl*). *Bars* illustrate the number and size of overlapping PSD-95 and VGLUT 1 puncta in dendritic segments normalized to the average values of control-infected neurons in each of five independent experiments (Mann-Whitney test (*, $p < 0.05$): number: ctrl, $n = 75$ dendritic segments; BRAG1-KD, $n = 56$, *, $p = 0.0067$; BRAG2-KD, $n = 60$, *, $p = 0.0096$; size: ctrl, $n = 75$; BRAG1-KD, $n = 56$, $p = 0.96$; BRAG2-KD, $n = 60$, *, $p = 0.0072$). *Error bars* indicate S.E. *Scale bars*, 10 μm.

the GluN2A/GluN2B ratio was much higher in the hippocampus than in the cortical cultures.

We also compared the relative frequencies of miniature amplitudes after knockdown of BRAG1 or BRAG2 using an equal number of events per cell and condition to prevent over-representation of single cells. The relative frequency distribution of mEPSCs in young neurons infected for BRAG1 RNAi at P0 (Fig. 9*A*) and of mature CA1 neurons lacking BRAG2 (Fig.
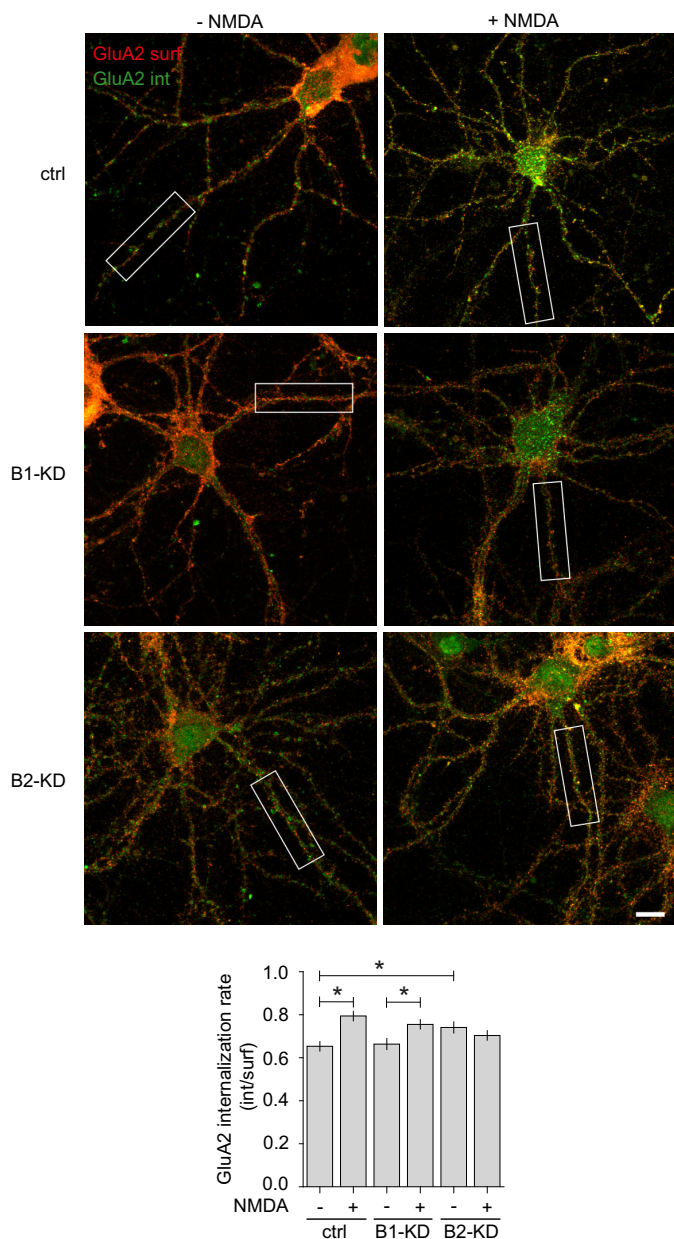
FIGURE 8. NMDA-triggered AMPAR internalization in mature neuronal cultures lacking BRAG1 or BRAG2. The endocytosis rate of the AMPAR subunit GluA2 with or without NMDA treatment was evaluated using a fluorescence internalization assay in rat hippocampal neurons (DIV24/25) infected at DIV15 with lentiviral vectors delivering shRNAs to BRAG1 (*B1-KD*), BRAG2 (*B2-KD*), or a control hairpin (*ctrl*). GluA2 internalization was calculated as the ratio between internalized (*int*) and surface-remaining (*surf*) GluA2 fluorescence signals in individual dendritic segments. *Top*, representative pictures of fluorescence signals in neurons and dendritic segments (indicated by *rectangles*). *Bottom*, bars showing average GluA2 internalization from four independent experiments (Mann-Whitney test (*, $p < 0.05$): ctrl − NMDA, $n = 66$ dendritic segments *versus* ctrl + NMDA, $n = 93$, *, $p < 0.0001$; BRAG1-KD −, $n = 90$ *versus* BRAG1-KD +, $n = 92$, *, $p = 0.023$; BRAG2-KD −, $n = 84$ *versus* BRAG2-KD +, $n = 97$, $p = 0.17$; BRAG1-KD − *versus* ctrl −, $p = 0.79$; BRAG2-KD − *versus* ctrl −, *, $p = 0.019$). *Error bars* indicate S.E. *Scale bar*, 10 μm.

9C) revealed a shift to smaller amplitudes as compared with uninfected neurons (Kolmogorov-Smirnov test, $p < 0.0001$). We cannot exclude that the amplitude shift results in a reduction of the mEPSCs to a level below the detection limit in a subset of synapses, thereby contributing to the reduced mEPSC frequencies. In contrast, BRAG2 RNAi at P0 did not affect

the relative frequency distribution of mEPSC amplitudes (Fig. 9B). Together, these results corroborate that signaling through BRAG1 and BRAG2 is critical at different points in development, although the expression of both BRAG1 and BRAG2 in mouse forebrain was detectable at P1 and increased steadily afterward (Fig. 9D). In addition, the altered amplitude spectra and the reduced mEPSC frequencies suggest that BRAG depletion reduced the strength and the number of synapses.

Effects of BRAG2 Depletion on the Properties of Evoked EPSCs in Mature Hippocampal CA1 Pyramidal Neurons—We next tested whether the increased GluN2B-mediated effects on Arf6 that we observed upon down-regulation of BRAG2 in cultured neurons (Fig. 6A) would manifest in a change of the synaptic NMDAR subunit composition in mature hippocampal CA1 pyramidal neurons of mice. To this end, we infected mice carrying loxP elements in the gene for BRAG2 (*Iqsec1$^{fl/fl}$* mice) (13) with a lentiviral Cre expression vector at 3–4 weeks of age. Two weeks later, isolated AMPAR and NMDAR currents were recorded from CA1 pyramidal neurons upon Schaffer collateral stimulation in acute slices (Fig. 10A). We did not observe any difference in the kinetic profile of NMDAR currents upon Cre infection (Fig. 10B; ctrl, $n = 14$ *versus* ΔBRAG2, $n = 7$; rise, $p = 0.38$; decay, $p = 0.57$). This result indicates that there was no increased participation of GluN1/N2B heterodimers in the synaptic NMDARs of cells lacking BRAG2 as this would have prolonged both the rise and decay of their currents (9, 35).

The ratio between the peak amplitudes of AMPAR and NMDAR currents was increased to some extent in BRAG2 knock-out cells as compared with controls (Fig. 10C; ctrl, $n = 14$ *versus* ΔBRAG2, $n = 7$; $p = 0.048$, Mann-Whitney test), suggesting a relative gain of AMPAR current and/or a relative loss of NMDAR current in mature CA1 neurons lacking BRAG2. A significant fraction of synapses on mature CA1 neurons contains functional NMDARs but lacks physiological AMPAR currents and is therefore called silent synapses (1, 30, 36–38). The CV was significantly different between AMPAR and NMDAR currents in uninfected but not in BRAG2 knock-out neurons (Fig. 10D; AMPAR *versus* NMDAR; ctrl, $n = 14$, $p = 0.0015$; ΔBRAG2, $n = 7$, $p = 0.20$), indicating a relative reduction in the number of silent synapses that may contribute to the increase in the AMPA/NMDA ratio. Paired pulse ratios were not altered by Cre infection (Fig. 10E; ctrl, $n = 6$ *versus* ΔBRAG2, $n = 9$; $p = 0.62$), suggesting no change in the release probability of glutamate. This allowed us to deduce the AMPAR and NMDAR quantal sizes from the relation of the mean EPSCs with their corresponding CV^{-2}, which served as a measure of the number of activated synapses (Fig. 10F). AMPAR and NMDAR quantal sizes were significantly reduced in cells lacking BRAG2 (ctrl, $n = 20$ *versus* ΔBRAG2, $n = 16$; $p = 0.025$ for AMPAR; ctrl, $n = 14$ *versus* ΔBRAG2, $n = 7$; $p = 0.018$ for NMDAR; linear regression F-test). Thus, CA1 neurons lacking BRAG2 had fewer AMPAR-silent synapses and lower AMPAR and NMDAR currents per Schaffer collateral synapse.
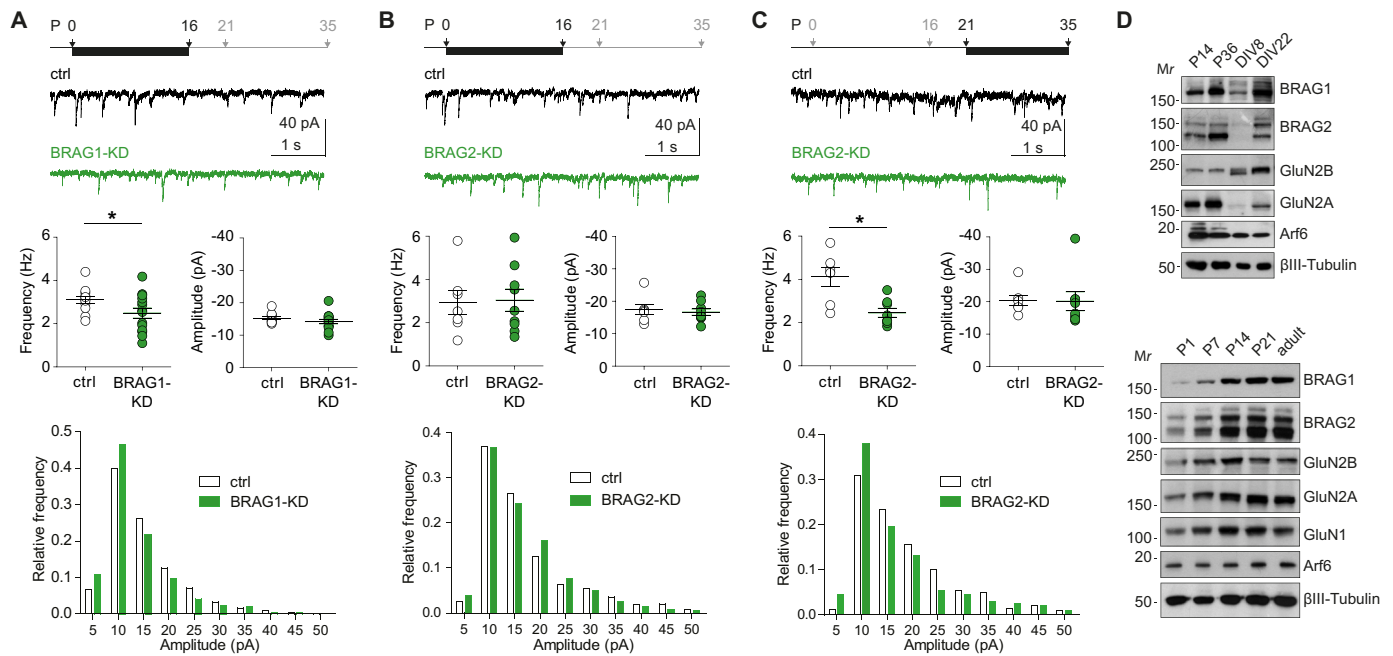
FIGURE 9. **Loss of BRAG1 or BRAG2 alters AMPAR mEPSC frequency and amplitude distribution in CA1 pyramidal neurons.** *A–C*, the impact of BRAG1 or BRAG2 signaling on synaptic transmission during development was assessed by recording of spontaneous AMPAR mEPSCs at a holding potential of −70 mV. Recordings were performed around P16 for P0-injected mice using viral constructs for shRNA to BRAG1 (*A*) or shRNA to BRAG2 (*B*) or after P35 for P21-injected mice using shRNA to BRAG2 (*C*). Example traces for uninfected (*ctrl*) and infected cells are shown below the experimental timelines indicating times of infection and experiment (*black arrows*). Data are plotted for mEPSC frequency and amplitude and reported as mean ± S.E. (*error bars*); *, $p < 0.05$ using Student's unpaired *t* test. Relative frequency distribution plots for 5-pA bins are shown on the *bottom* (amplitude values indicate the center of each bin). These plots contain data sets of an equal number of events per cell and condition to prevent overrepresentation of single cells. *D*, expression levels of NMDAR subunits, BRAGs, and Arf6 in postnatal mouse hippocampi and in rat cortical neuron cultures (*top*) as well as during mouse forebrain development (*bottom*). Shown are Western blots of nucleus-free tissue extracts and of neuronal culture homogenates adjusted to obtain comparable βIII-tubulin immunoreactivities.

Discussion

Here we report interactions between NMDARs and BRAG proteins that mediate an activity-dependent regulation of neuronal Arf6-GTP levels. We previously found that the AMPAR subunit GluA2 stimulates BRAG2 in the course of LTD triggered by metabotropic glutamate receptors (13). Thus, BRAG stimulation appears to represent a general function of ionotropic glutamate receptors, ensuring a tight link between synaptic activity and BRAG-mediated Arf6 activation.

Ligand-bound NMDA receptors stimulate the GEF activity of BRAG1 and BRAG2 by calcium influx and by the large intracellular domains of GluN2B and GluN2A. The GluN2 subunits recruit a differential set of GEFs for the small GTPases Ras and Rac1 as well (39–42). The fact that closely related GEFs associate with the C-terminal tails of GluN2A and GluN2B lends further support to the idea that gene duplication and paralog diversification increased the variety of postsynaptic signal transduction complexes (43). Quantitative mass spectrometry revealed that the numbers of BRAG1 and BRAG2 molecules per average PSD in adult rat cerebral cortex are in a similar range as that of NMDARs (around 10% of PSD-95), confirming their availability as postsynaptic binding partners (14). In the absence of BRAG1 or BRAG2, we frequently observed Arf6-GTP hydrolysis upon NMDAR stimulation. Thus, Arf6 is most likely regulated by synaptic pairs of GEFs and GTPase-activating proteins as shown for Rac1 (44). The NMDAR complex contains AGAP3, a GTPase-activating protein for Arf6 (45),

that may be a candidate GTPase-activating protein partner of BRAG2.

We identified short regions within the C-terminal tails of GluN2A and GluN2B that mediate an interaction with BRAGs and are critical for signaling from NMDARs to BRAGs *in vitro*. These regions may serve as targets to manipulate NMDAR-dependent Arf6 activation in neurons. The interaction between GluN2 subunits and BRAGs may involve additional binding sites and/or proteins. Furthermore, PSD-95 family members may stabilize or coordinate NMDAR-BRAG complexes.

An increase in the intracellular calcium concentration was required for NMDAR-BRAG signaling in HEK293 cells, and calcium promoted selective interactions between NMDARs and BRAGs. The calcium sensor calmodulin interacts with the IQ-like motif of BRAG1 (15) and BRAG2 (data not shown) only in the absence of calcium. Calcium-triggered release of calmodulin induced a conformational change in BRAG1 (15). The calcium-sensitive calmodulin binding may modulate the interactions of BRAGs with GluN2 subunits and thereby contribute to the regulation of NMDAR-BRAG signaling.

Our experiments in primary cortical neurons revealed that GluN2B-BRAG1 signaling is replaced by GluN2A-BRAG2 signaling over time. In young but not in mature cultures, we detected tonic GluN2B-BRAG1 signaling that may contribute to the Arf6-dependent morphological maturation of dendritic spines (18, 19) and/or to the relatively low plasticity threshold of young synapses (46). In mature neurons, NMDAR-depen-
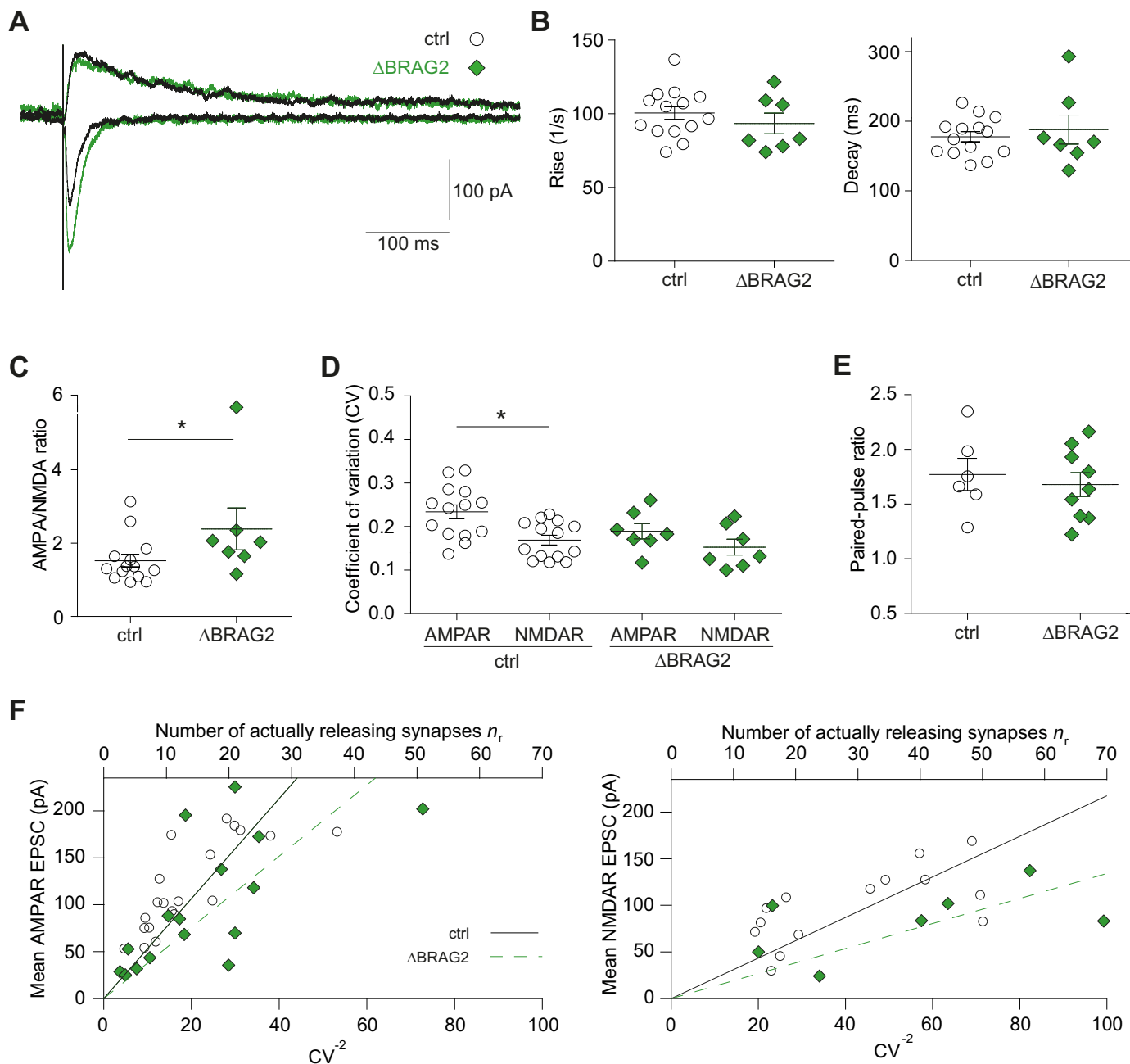
FIGURE 10. **Effects of BRAG2 depletion on evoked AMPAR and NMDAR currents in mature CA1 pyramidal neurons.** *A,* representative current traces to compare NMDAR decay (averages of 15 sweeps) recorded at −70 mV (AMPAR current) and following AMPAR blockade at +40 mV (NMDAR current) from uninfected (*ctrl*) and Cre-infected *green* CA1 pyramidal neurons (ΔBRAG2) in acute slices from mice homozygous for a floxed BRAG2 allele (*Iqsec1*$^{fl/fl}$) upon Schaffer collateral stimulation. *B,* rise and decay of NMDAR currents is unaffected and shown for individual neurons as marks and as mean ± S.E. (*error bars*) (15 repetitions per cell). *C,* AMPA/NMDA ratio is enhanced in infected neurons (15 repetitions per cell for AMPAR and NMDAR, respectively). *D,* CV of evoked NMDAR currents is smaller than CV of evoked AMPAR currents in uninfected but not in infected neurons (15 repetitions per cell for AMPAR and NMDAR, respectively). *E,* paired pulse ratio of evoked AMPAR currents (30 repetitions per cell). *F,* AMPAR (*left*) and NMDAR (*right*) average EPSC per cell *versus* corresponding CV^{-2} as a measure for number of stimulated synapses because release probability is unchanged (see *E*). Linear regressions through the origin indicate reduced AMPAR as well as NMDAR quantal sizes in infected neurons. The *upper x axes* illustrate (for release probability 0.3) that a larger number of actually releasing synapses needs to be activated upon BRAG2 deletion to evoke AMPAR and NMDAR currents with comparable amplitudes (15–30 repetitions per cell for AMPAR and 15 repetitions per cell for NMDAR). *, $p < 0.05$.

dent Arf6 activation relied on signaling through GluN2A and BRAG2 and was not induced by the endogenous excitation in the culture. Therefore, the incorporation of GluN2A into NMDARs affects not only the biophysical properties of their currents (4, 9, 35) but also restricts Arf6 activation to strong inputs. The tonic NMDAR-dependent Arf6 activation is shut down during development (Fig. 4*A*), although both GluN2B

and BRAG1 are present at mature synapses (9, 14, 35). AMPAR-BRAG2 signaling is blocked by tyrosine phosphorylation (13), and a posttranslational modification may prevent GluN2B-BRAG1 signaling at the mature stage as well. However, BRAG2 RNAi in mature neurons induced a return to GluN2B-BRAG1 signaling. Thus, recruitment of BRAG2 may impair GluN2B-BRAG1 signaling, *e.g.* by competitive binding to triheteromeric

NMDARs. Application of 300 nM Zn^{2+} reinstalled GluN2B-BRAG1 signaling in mature neurons as well, suggesting that GluN2A activation is required to maintain the low level of Arf6 activation. It will be interesting to see whether this phenomenon plays a role *in vivo*, *e.g.* during prolonged inactivity of synapses.

Measurements of AMPAR mEPSCs from hippocampal CA1 pyramidal neurons substantiated the importance of BRAG1 and BRAG2 at different stages of development. We found that BRAG1 plays a role in the maturation of synapses onto CA1 pyramidal neurons within the first 2 weeks of life. The mutations in the gene for BRAG1 identified in families with nonsyndromic X chromosome-linked intellectual disability result in a reduced GEF activity (22) and thus may affect GluN2B-BRAG1 signaling and the early postnatal development of synapses.

Although BRAG2 RNAi did not affect mEPSCs during the first 2 postnatal weeks, it resulted in a shift to smaller amplitudes and in a significantly reduced frequency of mEPSCs if applied at P21. In accord, knockdown of BRAG2 in mature neuronal cultures resulted in a decrease in the number as well as the size of glutamatergic synaptic contacts and elevated AMPAR internalization. Considering the tonic Arf6 activation through GluN2B-BRAG1 upon BRAG2 RNAi described above, these effects are in line with BRAG-dependent Arf6 activation mediating AMPAR internalization and synaptic depression (13, 15). Furthermore, targeted deletion of BRAG2 in hippocampal CA1 pyramidal neurons of P21 mice reduced the fraction of silent synapses as well as the quantal sizes of evoked AMPAR and NMDAR currents. Together, the loss of BRAG2 compromised the synaptic connections onto CA1 pyramidal neurons.

The formation of functional synapses is thought to involve an initial GluN2B-dependent limitation of AMPAR trafficking to synapses and a subsequent relief from synaptic suppression upon incorporation of GluN2A (7–9). BRAG2 depletion reverted the drop in Arf6 activity induced by the developmental GluN2 subunit switch without altering the NMDAR subunit composition and caused synapse weakening. Therefore, we propose that the down-regulation of the Arf6 activity induced by the incorporation of GluN2A contributes to the formation of mature synapses.

The coordinated transition of GluN2B-BRAG1 to GluN2A-BRAG2 signaling may be critical for synaptic selection because it ensures that the tonic synapse-suppressing Arf6 activity is switched off only at those connections with a strong or correlated neuronal activity, whereas others get eliminated. Tonic Arf6 activation may also contribute to metaplasticity based on an increased participation of GluN2B in NMDARs (46–49).

We previously identified a pathway through metabotropic glutamate receptors and AMPARs to stimulate BRAG2 and found that neither metabotropic glutamate receptor- nor NMDAR-dependent LTD could be induced in mature hippocampal CA1 neurons lacking BRAG2 (13). The GluN2A-BRAG2 signaling reported here may provide an explanation for the block of NMDAR-dependent LTD upon BRAG2 deletion. Conversely, the suppression of synaptic currents caused by the absence of BRAG2 may have prevented further depression upon LTD-related stimuli.

In summary, NMDARs, via their GluN2 subunits, consecutively stimulate BRAG1 and BRAG2 in the process of synapse maturation. It will be important to address the roles of these two pathways in homeostatic plasticity as well as in neurological disorders.

References

1. Hanse, E., Seth, H., and Riebe, I. (2013) AMPA-silent synapses in brain development and pathology. *Nat. Rev. Neurosci.* **14,** 839–850
2. Paoletti, P., Bellone, C., and Zhou, Q. (2013) NMDA receptor subunit diversity: impact on receptor properties, synaptic plasticity and disease. *Nat. Rev. Neurosci.* **14,** 383–400
3. Carmignoto, G., and Vicini, S. (1992) Activity-dependent decrease in NMDA receptor responses during development of the visual cortex. *Science* **258,** 1007–1011
4. Monyer, H., Burnashev, N., Laurie, D. J., Sakmann, B., and Seeburg, P. H. (1994) Developmental and regional expression in the rat brain and functional properties of four NMDA receptors. *Neuron* **12,** 529–540
5. Sheng, M., Cummings, J., Roldan, L. A., Jan, Y. N., and Jan, L. Y. (1994) Changing subunit composition of heteromeric NMDA receptors during development of rat cortex. *Nature* **368,** 144–147
6. Bellone, C., and Nicoll, R. A. (2007) Rapid bidirectional switching of synaptic NMDA receptors. *Neuron* **55,** 779–785
7. Hall, B. J., Ripley, B., and Ghosh, A. (2007) NR2B signaling regulates the development of synaptic AMPA receptor current. *J. Neurosci.* **27,** 13446–13456
8. Adesnik, H., Li, G., During, M. J., Pleasure, S. J., and Nicoll, R. A. (2008) NMDA receptors inhibit synapse unsilencing during brain development. *Proc. Natl. Acad. Sci. U.S.A.* **105,** 5597–5602
9. Gray, J. A., Shi, Y., Usui, H., During, M. J., Sakimura, K., and Nicoll, R. A. (2011) Distinct modes of AMPA receptor suppression at developing synapses by GluN2A and GluN2B: single-cell NMDA receptor subunit deletion *in vivo*. *Neuron* **71,** 1085–1101
10. Sheng, M., and Hoogenraad, C. C. (2007) The postsynaptic architecture of excitatory synapses: a more quantitative view. *Annu. Rev. Biochem.* **76,** 823–847
11. Murphy, J. A., Jensen, O. N., and Walikonis, R. S. (2006) BRAG1, a Sec7 domain-containing protein, is a component of the postsynaptic density of excitatory synapses. *Brain Res.* **1120,** 35–45
12. Sakagami, H., Sanda, M., Fukaya, M., Miyazaki, T., Sukegawa, J., Yanagisawa, T., Suzuki, T., Fukunaga, K., Watanabe, M., and Kondo, H. (2008) IQ-ArfGEF/BRAG1 is a guanine nucleotide exchange factor for Arf6 that interacts with PSD-95 at postsynaptic density of excitatory synapses. *Neurosci. Res.* **60,** 199–212
13. Scholz, R., Berberich, S., Rathgeber, L., Kolleker, A., Köhr, G., and Kornau, H. C. (2010) AMPA receptor signaling through BRAG2 and Arf6 critical for long-term synaptic depression. *Neuron* **66,** 768–780

14. Lowenthal, M. S., Markey, S. P., and Dosemeci, A. (2015) Quantitative mass spectrometry measurements reveal stoichiometry of principal post-synaptic density proteins. *J. Proteome Res.* **14,** 2528 –2538

15. Myers, K. R., Wang, G., Sheng, Y., Conger, K. K., Casanova, J. E., and Zhu, J. J. (2012) Arf6-GEF BRAG1 regulates JNK-mediated synaptic removal of GluA1-containing AMPA receptors: a new mechanism for nonsyndromic X-linked mental disorder. *J. Neurosci.* **32,** 11716 –11726

16. Donaldson, J. G. (2003) Multiple roles for Arf6: sorting, structuring, and signaling at the plasma membrane. *J. Biol. Chem.* **278,** 41573– 41576

17. Humphreys, D., Davidson, A. C., Hume, P. J., Makin, L. E., and Koronakis, V. (2013) Arf6 coordinates actin assembly through the WAVE complex, a mechanism usurped by *Salmonella* to invade host cells. *Proc. Natl. Acad. Sci. U.S.A.* **110,** 16880 –16885

18. Choi, S., Ko, J., Lee, J. R., Lee, H. W., Kim, K., Chung, H. S., Kim, H., and Kim, E. (2006) ARF6 and EFA6A regulate the development and maintenance of dendritic spines. *J. Neurosci.* **26,** 4811– 4819

19. Kim, Y., Lee, S. E., Park, J., Kim, M., Lee, B., Hwang, D., and Chang, S. (2015) ADP-ribosylation factor 6 (ARF6) bidirectionally regulates dendritic spine formation depending on neuronal maturation and activity. *J. Biol. Chem.* **290,** 7323–7335

20. Zheng, N., Jeyifous, O., Munro, C., Montgomery, J. M., and Green, W. N. (2015) Synaptic activity regulates AMPA receptor trafficking through different recycling pathways. *Elife* **4,** e06878

21. Donaldson, J. G., and Jackson, C. L. (2011) ARF family G proteins and their regulators: roles in membrane transport, development and disease. *Nat. Rev. Mol. Cell Biol.* **12,** 362–375

22. Shoubridge, C., Tarpey, P. S., Abidi, F., Ramsden, S. L., Rujirabanjerd, S., Murphy, J. A., Boyle, J., Shaw, M., Gardner, A., Proos, A., Puusepp, H., Raymond, F. L., Schwartz, C. E., Stevenson, R. E., Turner, G., *et al.* (2010) Mutations in the guanine nucleotide exchange factor gene IQSEC2 cause nonsyndromic intellectual disability. *Nat. Genet.* **42,** 486 – 488

23. Schall, T. J., Lewis, M., Koller, K. J., Lee, A., Rice, G. C., Wong, G. H., Gatanaga, T., Granger, G. A., Lentz, R., Raab, H., Kohr, W. J., and Goeddel, D. V. (1990) Molecular cloning and expression of a receptor for human tumor necrosis factor. *Cell* **61,** 361–370

24. Dittgen, T., Nimmerjahn, A., Komai, S., Licznerski, P., Waters, J., Margrie, T. W., Helmchen, F., Denk, W., Brecht, M., and Osten, P. (2004) Lentivirus-based genetic manipulations of cortical neurons and their optical and electrophysiological monitoring *in vivo*. *Proc. Natl. Acad. Sci. U.S.A.* **101,** 18206 –18211

25. Xu, X. M., Yoo, M. H., Carlson, B. A., Gladyshev, V. N., and Hatfield, D. L. (2009) Simultaneous knockdown of the expression of two genes using multiple shRNAs and subsequent knock-in of their expression. *Nat. Protoc.* **4,** 1338 –1348

26. Lois, C., Hong, E. J., Pease, S., Brown, E. J., and Baltimore, D. (2002) Germline transmission and tissue-specific expression of transgenes delivered by lentiviral vectors. *Science* **295,** 868 – 872

27. Lock, M., Alvira, M., Vandenberghe, L. H., Samanta, A., Toelen, J., Debyser, Z., and Wilson, J. M. (2010) Rapid, simple, and versatile manufacturing of recombinant adeno-associated viral vectors at scale. *Hum. Gene. Ther.* **21,** 1259 –1271

28. Santy, L. C., and Casanova, J. E. (2001) Activation of ARF6 by ARNO stimulates epithelial cell migration through downstream activation of both Rac1 and phospholipase D. *J. Cell Biol.* **154,** 599 – 610

29. Ippolito, D. M., and Eroglu, C. (2010) Quantifying synapses: an immunocytochemistry-based assay to quantify synapse number. *J. Vis. Exp.* e2270

30. Kerchner, G. A., and Nicoll, R. A. (2008) Silent synapses and the emergence of a postsynaptic mechanism for LTP. *Nat. Rev. Neurosci.* **9,** 813– 825

31. Paoletti, P., Ascher, P., and Neyton, J. (1997) High-affinity zinc inhibition

32. Choi, Y. B., and Lipton, S. A. (1999) Identification and mechanism of action of two histidine residues underlying high-affinity Zn^{2+} inhibition of the NMDA receptor. *Neuron* **23,** 171–180

33. Paoletti, P., Perin-Dureau, F., Fayyazuddin, A., Le Goff, A., Callebaut, I., and Neyton, J. (2000) Molecular organization of a zinc binding N-terminal modulatory domain in a NMDA receptor subunit. *Neuron* **28,** 911–925

34. Hansen, K. B., Ogden, K. K., Yuan, H., and Traynelis, S. F. (2014) Distinct functional and pharmacological properties of Triheteromeric GluN1/GluN2A/GluN2B NMDA receptors. *Neuron* **81,** 1084 –1096

35. Rauner, C., and Köhr, G. (2011) Triheteromeric NR1/NR2A/NR2B receptors constitute the major *N*-methyl-D-aspartate receptor population in adult hippocampal synapses. *J. Biol. Chem.* **286,** 7558 –7566

36. Liao, D., Hessler, N. A., and Malinow, R. (1995) Activation of postsynaptically silent synapses during pairing-induced LTP in CA1 region of hippocampal slice. *Nature* **375,** 400 – 404

37. Isaac, J. T., Nicoll, R. A., and Malenka, R. C. (1995) Evidence for silent synapses: implications for the expression of LTP. *Neuron* **15,** 427– 434

38. Takumi, Y., Ramírez-León, V., Laake, P., Rinvik, E., and Ottersen, O. P. (1999) Different modes of expression of AMPA and NMDA receptors in hippocampal synapses. *Nat. Neurosci.* **2,** 618 – 624

39. Krapivinsky, G., Krapivinsky, L., Manasian, Y., Ivanov, A., Tyzio, R., Pellegrino, C., Ben-Ari, Y., Clapham, D. E., and Medina, I. (2003) The NMDA receptor is coupled to the ERK pathway by a direct interaction between NR2B and RasGRF1. *Neuron* **40,** 775–784

40. Li, S., Tian, X., Hartley, D. M., and Feig, L. A. (2006) Distinct roles for Ras-guanine nucleotide-releasing factor 1 (Ras-GRF1) and Ras-GRF2 in the induction of long-term potentiation and long-term depression. *J. Neurosci.* **26,** 1721–1729

41. Kiraly, D. D., Lemtiri-Chlieh, F., Levine, E. S., Mains, R. E., and Eipper, B. A. (2011) Kalirin binds the NR2B subunit of the NMDA receptor, altering its synaptic localization and function. *J. Neurosci.* **31,** 12554 –12565

42. Schwechter, B., Rosenmund, C., and Tolias, K. F. (2013) RasGRF2 Rac-GEF activity couples NMDA receptor calcium flux to enhanced synaptic transmission. *Proc. Natl. Acad. Sci. U.S.A.* **110,** 14462 –14467

43. Ryan, T. J., Kopanitsa, M. V., Indersmitten, T., Nithiananthrajah, J., Afinowi, N. O., Pettit, C., Stanford, L. E., Sprengel, R., Saksida, L. M., Bussey, T. J., O'Dell, T. J., Grant, S. G., and Komiyama, N. H. (2013) Evolution of GluN2A/B cytoplasmic domains diversified vertebrate synaptic plasticity and behavior. *Nat. Neurosci.* **16,** 25–32

44. Um, K., Niu, S., Duman, J. G., Cheng, J. X., Tu, Y. K., Schwechter, B., Liu, F., Hiles, L., Narayanan, A. S., Ash, R. T., Mulherkar, S., Alpadi, K., Smirnakis, S. M., and Tolias, K. F. (2014) Dynamic control of excitatory synapse development by a Rac1 GEF/GAP regulatory complex. *Dev. Cell* **29,** 701–715

45. Oku, Y., and Huganir, R. L. (2013) AGAP3 and Arf6 regulate trafficking of AMPA receptors and synaptic plasticity. *J. Neurosci.* **33,** 12586 –12598

46. Yashiro, K., and Philpot, B. D. (2008) Regulation of NMDA receptor subunit expression and its implications for LTD, LTP, and metaplasticity. *Neuropharmacology* **55,** 1081–1094

47. Kirkwood, A., Rioult, M. C., and Bear, M. F. (1996) Experience-dependent modification of synaptic plasticity in visual cortex. *Nature* **381,** 526 –528

48. Abraham, W. C., and Bear, M. F. (1996) Metaplasticity: the plasticity of synaptic plasticity. *Trends Neurosci.* **19,** 126 –130

49. Lee, M. C., Yasuda, R., and Ehlers, M. D. (2010) Metaplasticity at single glutamatergic synapses. *Neuron* **66,** 859 – 870

50. Palmer, I., and Wingfield, P. T. (2004) Preparation and extraction of insoluble (inclusion-body) proteins from *Escherichia coli*. *Curr. Protoc. Protein Sci.* Chapter 6, Unit 6.3

Subunit-selective *N*-Methyl-d-aspartate (NMDA) Receptor Signaling through Brefeldin A-resistant Arf Guanine Nucleotide Exchange Factors BRAG1 and BRAG2 during Synapse Maturation

Mohammad Nael Elagabani, Dusica Brisevac, Michael Kintscher, Jörg Pohle, Georg Köhr, Dietmar Schmitz and Hans-Christian Kornau

Access the most updated version of this article at doi: 10.1074/jbc.M115.691717

Alerts:
- When this article is cited
- When a correction for this article is posted

Click here to choose from all of JBC's e-mail alerts

This article cites 48 references, 18 of which can be accessed free at
http://www.jbc.org/content/291/17/9105.full.html#ref-list-1